UCRL-9787

University of California

Ernest O. Lawrence Radiation Laboratory

DISPERSED-PHASE DISTRIBUTION PATTERNS IN LIQUID-LIQUID AGITATION

TWO-WEEK LOAN COPY

This is a Library Circulating Copy which may be borrowed for two weeks. For a personal retention copy, call Tech. Info. Division, Ext. 5545

DISCLAIMER

This document was prepared as an account of work sponsored by the United States Government. While this document is believed to contain correct information, neither the United States Government nor any agency thereof, nor the Regents of the University of California, nor any of their employees, makes any warranty, express or implied, or assumes any legal responsibility for the accuracy, completeness, or usefulness of any information, apparatus, product, or process disclosed, or represents that its use would not infringe privately owned rights. Reference herein to any specific commercial product, process, or service by its trade name, trademark, manufacturer, or otherwise, does not necessarily constitute or imply its endorsement, recommendation, or favoring by the United States Government or any agency thereof, or the Regents of the University of California. The views and opinions of authors expressed herein do not necessarily state or reflect those of the United States Government or any agency thereof or the Regents of the University of California.

Research and Development

UCRL-9787
UC-4 Chemistry
TID-4500 (17th ed.)

UNIVERSITY OF CALIFORNIA

Lawrence Radiation Laboratory
Berkeley, California

Contract No. W-7405-eng-48

DISPERSED-PHASE DISTRIBUTION PATTERNS IN LIQUID-LIQUID AGITATION

Lawrence H. Weiss, J. Leonard Fick, Robert H. Houston,
and Theodore Vermeulen

September 6, 1962

Printed in USA. Price $2.00. Available from the
Office of Technical Services
U. S. Department of Commerce
Washington 25, D.C.

DISPERSED-PHASE DISTRIBUTION PATTERNS IN LIQUID-LIQUID AGITATION

Contents

Abstract v

I. Introduction 1

A. Interfacial-Area Measurement 2

B. Bulk Homogeneity of Two-Phase Systems 4

1. Solid-Liquid Systems 4

2. Liquid-Liquid Systems 8

II. Statement of the Problem 13

III. A. Two-Parameter Model for Dispersion 14

A. Preliminary Considerations 14

B. Analysis for κ 19

C. Analysis for h_B 22

D. Behavior of the Model Parameters 24

IV. Experimental Program

A. Apparatus 32

B. Sampling Probe 34

C. Materials and Physical Variables 35

D. Operating Procedure 40

V. Results and Discussion

A. Observed Distribution Profiles 41

B. Computational Methods and Results 41

C. Correlations for the Parameters

1. Result for κ 60

2. Result for h_B 63

D. Conditions for the Occurrence of Kappa Control 64

E. Comparison With Results of Other Investigators 69

VI. Applications 71

A. Testing an Existing Process 71

B. Design of Equipment 72

VII. Conclusions 74

Acknowledgments 76

Appendices

1. Computation Procedure and Tabulated Results 77

2. Nomenclature 83

References 86

DISPERSED-PHASE DISTRIBUTION PATTERNS IN LIQUID-LIQUID AGITATION

Lawrence H. Weiss, Jr., J. Leonard Fick, Robert H. Houston, and Theodore Vermeulen

Lawrence Radiation Laboratory and Department of Chemical Engineering
University of California
Berkeley, California

September 6, 1962

ABSTRACT

The distribution of dispersed phase throughout a baffled tank was measured for a number of immiscible liquid pairs over a range of turbulent mixing conditions. The volume-fraction of dispersed phase, ϕ_s, was found to be independent of radial position. The variation of ϕ_s over the height of the agitator followed an exponential distribution function:

$$\phi_s = \phi_{max} \; e^{-\kappa(h - h_B)}$$

The parameter κ represents the extent of inhomogeneity within the emulsion and is correlated by:

$$\kappa = 88 \left[\left(\frac{N^2 L^2 \bar{\rho}}{d_p g \, (1 - \phi) \, |\Delta \rho|} \right)^3 \left(\frac{N L d_p \bar{\rho}}{\mu_m} \right) \left(\frac{LW}{TH} \right)^{3/2} \right]^{-2/7}$$

The parameter h_B is the fractional tank-height of the boundary between the stagnant layer (if any) of the dispersible phase and the emulsified mixture. It has been correlated by

$$\frac{h_B}{\bar{\phi}} = -1.39 \log_{10} \left[\left(\frac{N^2 L^3 \bar{\rho}}{\sigma} \right) \left(\frac{LW}{TH} \right)^{0.7} \right] + 2.31 ,$$

with the limitation that $\bar{\phi} \geqslant h_B \geqslant 0$. A criterion for complete bulk dispersion is obtained by setting the argument of the logarithm equal to 38.

The inadequacies of single-parameter criteria are discussed. The present results are compared with other studies of homogeneity in both liquid-liquid and liquid-solid systems. The available results are shown to be consistent for each system.

DISPERSED-PHASE DISTRIBUTION PATTERNS IN LIQUID-LIQUID AGITATION

Lawrence H. Weiss, Jr., J. Leonard Fick, Robert H. Houston, and Theodore Vermeulen

Lawrence Radiation Laboratory and Department of Chemical Engineering
University of California
Berkeley, California

September 6, 1962

I. INTRODUCTION

Bringing heterogeneous phases into contact in agitators is among the oldest of process operations, but there are still many areas of application for which performance requirements cannot be satisfactorily predicted. Mixing equipment generally requires a maximum thoroughness of homogenization and interphase contacting in each local region for peak performance. This study, together with previous work at this laboratory,[2,7,16,22,24] was made to investigate the problem of attaining effective multiphase mixing with conventional agitation equipment.

Because mixing of immiscible liquids is usually undertaken to allow mass transfer between the phases, three primary objectives of the process can be identified:

(a) to provide homogeneous bulk mixing, which ensures adequate contacting of the intersuspended phases;

(b) to provide a turbulent field around and within the droplets, which directly reduces resistance to mass transfer; and

(c) to provide a large interfacial area, which also serves to promote interphase transport.

In terms of the fluid mechanics of the process, these three goals are

closely related; nevertheless, the successful attainment of any one of them does not necessarily indicate satisfactory levels for the other two. The criteria for obtaining homogeneity are important both to assure uniform interphase contact and as guides to desirable levels of turbulence and drop size. It should also be noted that bulk homogeneity is a primary objective in the suspending of solids and the blending of miscible liquids.

Previous work at this laboratory and elsewhere in the field of liquid-liquid agitation has been concerned with measuring and predicting interfacial area and agitator-power requirements.

Satisfactory correlations have been established for power input as a function of the impeller Reynolds number and vessel geometry, as has been indicated in a very recent survey by Hyman.[4] While the power delivered to the fluid does not all produce turbulence, studies by Sachs,[20] and Yamomoto and Kawahigasi,[28] show a relation between impeller-tip velocity and the turbulent velocity fluctuations. The earlier work at this laboratory by Fick and coworkers,[2] and Rea and co-workers,[16] showed that the same power correlations hold for heterogeneous liquid systems as for homogeneous liquids, and this provided preliminary information about the production of turbulence in these systems. The only modifications to the well-known correlations for single-phase systems of Rushton et al.[18,19] were the introduction of volumetric-mean physical properties for the heterogeneous systems.

A. Interfacial Area Measurement

The study of interfacial area in heterogenous fluid dispersions was investigated with use of a light-transmission probe, by Langlois and co-workers.[7,24] The probe measures the transmission of an emulsion of two

colorless fluids and compares this with the transmission of light through the continuous phase alone. The photoelectric measurements were calibrated with actual drop diameters by use of high-speed photography. Subsequent investigations by Rea et al.,[16] Fick et al.,[2] and Vanderveen,[22] have resulted in correlations of drop diameter with physical and geometric variables, including the bulk-average volume fraction of dispersed phase $\bar{\phi}$, and the variables entering into the Weber number N_{We}. Somewhat different results were found by Rodger and co-workers[17,21] involving a smaller dependence upon N_{We}, and including a settling-time ratio to be determined empirically for each pair of fluids. From a consideration of the probe locations used by each, it is apparent that more coalescence occurred in Rodger's systems than in those of Langlois.

The recent work by Vanderveen[22] extended the earlier studies by Fick, Rea, and Langlois to take quantitative account of coalescence in the liquid-liquid systems. Vanderveen found that the coalescence of drops could be best accounted for by a linear relation that adds an increment to the average droplet diameter at points remote from the impeller tip:

$$d_i = d_0 + b'_{0-i} \Delta'_i , \qquad (1)$$

where d_i = mean droplet diameter at point i, d_0 = mean droplet diameter at the impeller tip, b'_{0-i} = a geometric constant, showing probe location, and Δ'_i = the coalescence correction factor.

The values of b'_{0-i} are tabulated for several different locations by Vanderveen, and the other terms are correlated with the physical properties of the liquids and the agitator geometry by the following relations:

$$d_0 = 0.055\ L\ f(\phi)\ N_{We}^{-0.60}\ , \qquad (2)$$

and

$$\Delta_1' = L\ N_{We}^{-0.45}\ N_{Re}^{0.25}\ \psi^{-0.70}\ \phi^{0.30}\ , \qquad (3)$$

where L = impeller diameter, $f(\phi) = 1 + 2.5\ \phi$. N_{Re} = impeller Reynolds number, and ψ = a function of phase viscosities and volume fractions. While the exact form of the correlations is open to further investigation including possible use of a settling-time term, Vanderveen's study shows that coalescence in areas of an agitator remote from the impeller can be significant in predicting performance.

B. Bulk Homogeneity of Two-Phase Systems

As mentioned above, an equally important criterion for evaluating the performance of an agitator is the degree of bulk homogeneity attained in the resulting emulsion or suspension. The need to keep two phases completely intersuspended, thus avoiding any dead space, is often of critical economic importance. If any portion of the dispersible phase is not dispersed in a reasonably uniform manner, the effect is essentially that of removing this portion and the volume it occupies from the agitator, usually with a detrimental effect. Fro this reason, homogeneity has been investigated over a substantial range of conditions, as summarized below.

1. Solid-Liquid Systems

A number of studies have been published concerning the suspension of solids in liquids. In an early work, Hixson and Tenney investigated suspensions of sand both in water and in sucrose-water solutions.[3] Since the vessel they

used was unbaffled and open at the top, a vortex was present in all of the runs; this limits the applicability of their results to our study. However, the concept of a "mixing index" as a characterization of homogeneity was proposed in that paper and has since been widely adopted. Homogeneity was investigated by drawing samples from various locations in the vessel and comparing their compositions with the known over all composition. These measurements were used to compute local values of "mixing index", which were then averaged to define empirically the overall degree of homogeneity in the agitator.

In terms of the notation used here, the Hixson-Tenney definition would be

$$I_m = \frac{100}{q} \sum_{j=1}^{q} \frac{\phi_{s,j}}{\bar{\phi}} , \qquad (4)$$

where q samples are taken of the local volume fraction ϕ_s. It is obvious that when bulk homogeneity is not approached, one phase will predominate in certain regions. The experimenter must either choose to compute the ratio for the component which gives a values less than unity (100%), or else confine his measurements to that portion of the vessel richer in continuous-phase materials. This definition also gives a discontinuity at 100% mixing index in the plot of mixing index against local volume fraction ϕ_s, for all systems except the special case of $\bar{\phi} = 0.50$. This results in different values for the "mixing index" for equal, small departures from a value of 100%.

In other early studies, White and co-worders measured concentration profiles for solid-liquid systems.[26,27] In more recent work, Nagata et al.

have photographed such suspensions;[9,10] they have established that mass-transfer rates are optimal (relative to power input) when all the solid particles have just been suspended,[11] thus obviating the need to attain complete bulk homogeneity for this particular case. In a further study, Kneule confirmed that mass-transfer rates increase only slightly when impeller speed is raised beyond the conditions necessary for complete suspension of the solids.[5]

This work guided Zwietering to investigate extensively the conditions which will just suspend all the particles.[29] His study covered a large range of liquid and solid physical properties in addition to several different agitator geometries in fully baffled vessels. Using the value of 1.5 given for turbines as the exponent of the geometric ratio, Zwietering's result is:

$$N_{Re}^{0.1} N_{Fr}^{0.45} \left(\frac{L}{d_p}\right)^{0.2} = K\left(\frac{T}{L}\right)^{1.5} B^{0.13} , \quad (5)$$

with the Froude group modified here to include the ratio $\rho_c \Delta\rho$. Therefore, $N_{Fr} = N^2 L \rho_c / g\Delta\rho$; and $N_{Re} = NL^2 \rho_c/\mu_c$. The value of the constant K depends upon the distance between the impeller and the tank bottom; B is the weight-percent of solids. Zwietering's result does not predict homogeneity, but only the first complete suspension of particles. In his runs, the maximum fraction of solids was 30% by weight.

Studies of the "critical speed" at which solid-liquid systems reach constant composition at or above the impeller in baffled vessels have been made by Oyama and Endoh.[13] Their correlation is independent of solids loading, but the range of this variable was limited to about 1% by weight or lower. The criterion determined by this was

$$N_{Fr}^{0.5}\left(\frac{L}{d_p}\right)^{0.17} = K\left(\frac{T}{L}\right). \qquad (6)$$

For the same standard of homogeneity in solid suspensions, but in an unbaffled tank, Pavlushenko and co-workers found the "critical speed" relation to be[14]

$$N_{Re}^{-0.2}\ N_{Fr}^{0.6}\left(\frac{L}{d_p}\right)^{0.4} = K\left(\frac{T}{L}\right)^{1.9}. \qquad (7)$$

Since this study was made in a single tank, the tank diameter is present only as a result of dimensional analysis. These workers found that this correlation applied for solids loading from 20 to 50% by weight, and that the "critical speed" was proportional to the solids loading in the range below 20%.

In yet another study of optimum stirrer speed for solids suspension in unbaffled tanks, Nagata and co-workers used the criterion of all particles being in suspension.[11] This correlation for optimum speed was

$$N_{Re}^{-0.12}\ N_{Fr}^{0.56}\left(\frac{L}{d_p}\right)^{0.33} = K\ \frac{T}{L}\left(\frac{V_p}{V_p'}\right)^{0.7}, \qquad (8)$$

where the ratio (V_p/V_p') measures the average departure from sphericity of the solid particles.

Recent work by Weisman and Efferding supports some of the foregoing results.[25] They found it necessary to consider the expansion of the slurry bed to occupy the entire column of the mixing vessel, as well as the initial suspension of particles. In a baffled vessel, once all the solids are suspended, the slurry is essentially uniform in any plane parallel to the bottom

of the tank. Except for the volume just below the slurry/clear-liquid "interface", the slurry appears to have a linear pressure-depth relation. These authors therefore concluded that the major design criterion is the fraction of the total volume occupied by the slurry. The correlation they proposed for the fractional height of the slurry was

$$h_s = (\text{const}) + \ln\left[N_{Re}^{-0.23}\, N_{Fr}^{0.46}\left(\frac{L}{d_p}\right)^{0.46}\left(\frac{L}{T}\right)^{0.81}\bar{\phi}^{-0.38}\, h_s^{-0.31}\right] \tag{9}$$

where h_s is the fractional height of the slurry, and $\bar{\phi}$ the overall volume-fraction of solids in the tank.

2. Liquid-Liquid Systems

The first attempt to apply quantitative standards of homogeneity to heterogeneous liquid systems was in the study by Miller and Mann.[8] The Hixson and Tenney "mixing index" method was applied in an unbaffled tank by diphoning out small samples under steady-state dynamic conditions. When relative volume-fractions were determined after the samples had settled, the inherent deficiencies in this definition, mentioned earlier, became evident. These workers presented no general correlation of variables, but concluded that power input was the major factor governing homogeneity, while the geometric and physical variables were of secondary importance. When "mixing index" was plotted against power input, an optimum generally occurred at 1 to 2 hp/1000 gal. Limited data showed that scale-up at constant "mixing index" could be achieved by using equal power input per unit volume.

In more recent studies, Nagata and co-workers investigated the impeller speed necessary to cause complete intersuspension of the dispersible phase.[12] The optimum turbine diameter was determined to be $L = T/3$. Other variables considered were the effects of various types of baffling and the shape of the vessel bottom. The correlation established for the liquid properties is

$$N_{min} = A \left(\frac{\mu_d}{\rho_c} \right)^{0.11} \left(\frac{\Delta\rho}{\rho_c} \right)^{0.26} , \tag{10}$$

where A is a function of geometrical factors. Although use of this minimum impeller speed will ensure avoiding a separate layer of dispersible phase, it does not ensure bulk homogeneity.

An extensive study of conditions for uniformity in heterogeneous liquid systems was carried out by Pavlushenko and Yanishevskii.[15] The measurements were made in a single 30-cm-diam round-bottom flask with turbine and propeller-type impellers under both baffled and unbaffled conditions. A vortex was present in all the unbaffled runs. Light-transmission measurements were used to determine the approach to homogeneity. The impeller speed required for complete bulk mixing increased with impeller distance from the static interface; the overall volume-fraction of dispersed phase had only a negligible effect in the range of $0.1 < \overline{\phi} < 0.7$. The result of this work in baffled tanks with turbine-type impellers is

$$N_{Re}^{0.10} \, N_{Fr}^{0.30} \, N_{We}^{0.15} = 2.85 \left(\frac{\mu_d}{\mu_c} \right)^{0.04} \left(\frac{\Delta \rho}{\rho_c} \right)^{0.08} \left(\frac{T}{L} \right)^{0.92} , \tag{11}$$

where, here, $N_{Fr} = N^2L/g$. A total of seven liquid pairs was employed in the study, allowing the ratios used in Eq. (11) to vary over a substantial range.

In a preliminary study at this laboratory by Fick,[2] the definition of "mixing index" was revised from that originally proposed by Hixson and Tenney. In order to provide for a continuous slope at 100% mixing index, and to indicate equal departures from bulk homogeneity for equal deviations immediately above and below the mean volume-fraction in systems where the latter is other than 0.50, the following definition of mixing number, M.N., was proposed:

$$\frac{200 - (\text{M.N.})}{(\text{M.N.})} = \frac{(1 - \phi_s)\overline{\phi}}{\phi_s(1 - \overline{\phi})} . \qquad (12)$$

Using this relation, the mixing number can vary from 0 to 200; then the mixing index, i_m, is chosen as either (200 - M.N.) or (M.N.), whichever results in a value for $i_m \leq 100$. This relation is illustrated in Fig. 1, where the functional symmetry is apparent. As in the work of other investigators, Fick defines an experimental overall mixing-index value, EMI or I_m, as the linear average of the individual point values, i_m:

$$\text{EMI} = I_m = \frac{1}{q} \sum_{j=1}^{q} i_{m,j} . \qquad (13)$$

As an initial basis for correlating EMI with the physical and geometric variables, a dimensionless group based on the Newtonian settling velocity of a particle in a turbulent field was proposed by Fick. Basing his final result on the empirical knowledge that complete bulk mixing is highly improbable, he presented a correlation of the normal probability of EMI vs the logarithm of the "settling group". This can be represented as

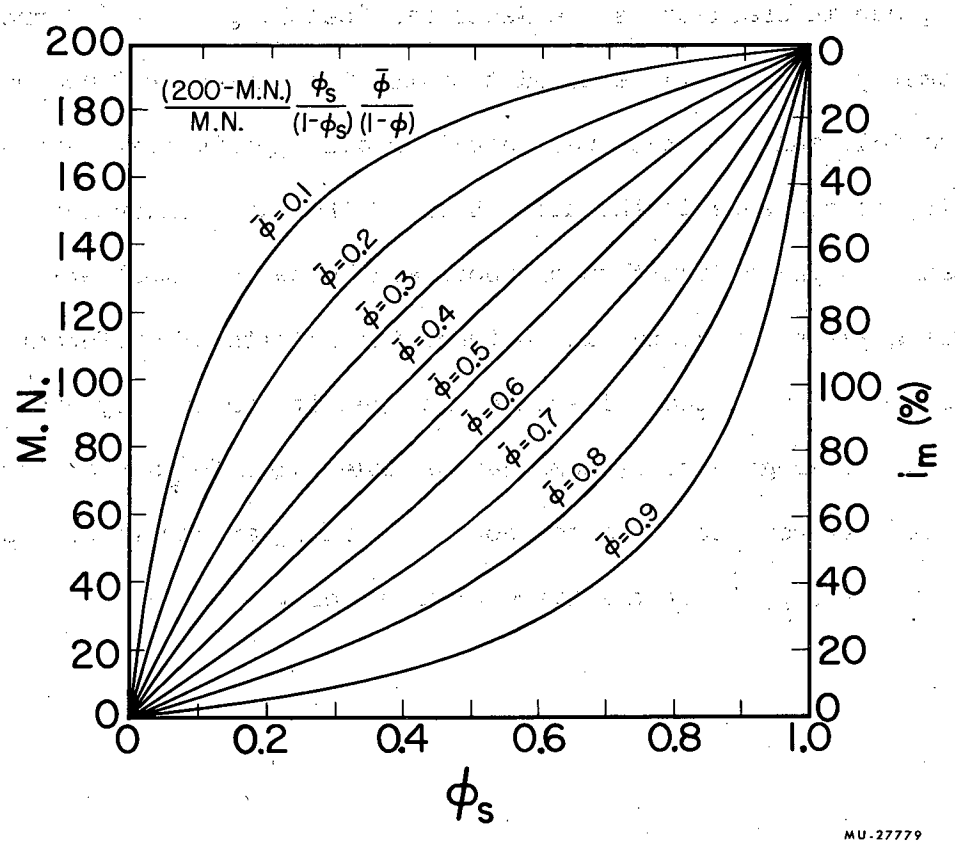

Fig. 1. Mixing index as a function of mixing number.

$$\text{prob}(\text{EMI}) = (a + b)\ \ell n \left[\frac{NL\ \bar{\rho}^{0.5}}{(|\Delta\ \rho\ |gd_p)^{0.5}} \cdot \frac{LW}{TH} \right], \tag{14}$$

where the group in brackets is the Newtonian "settling group," corrected for system geometry. It should be noted that the tank diameter T and height H were not varied, and that they were equal in all experiments. Further, all of the sampling points were in the upper half of the tank, under the assumption of a symmetry in phase distribution above and below the impeller.

The greatest discrepancies between the results of different investigators seem to occur in the criteria of homogeneity which they chose. Since the mixing of heterogeneous systems can be undertaken for a wide variety of reasons, the different criteria for complete mixing appear to be based upon different specific goals of the dispersion process.

II. STATEMENT OF THE PROBLEM

A criterion for evaluating mixer performance that is not based upon specific processing objectives or arbitrary standards of uniformity would be of greater use in the design of interphase contacting equipment. Since previous investigations have shown the limitations of a single-parameter description of homogeneity, this study was undertaken to examine more fully the fundamental problem of characterizing the dispersed-phase distribution in immiscible liquid mixtures. By establishing a valid model for such dispersions and developing correlations for all its parameters with the design variables, progress will be effected toward rational performance criteria and valid design procedures.

III. A TWO-PARAMETER MODEL FOR DISPERSIONS

Preliminary visual observation and measurement of dispersed systems indicate the existence of two types of inhomogeneity, which do not seem to be directly related to one another in most cases: (a) vertical inhomogeneity within the emulsified continuous phase, and (b) an undispersed second phase present as a discrete layer. These two types of inhomogeneity reflect the fundamental duality of the dispersing process. The first type is a result of insufficient circulation and turbulence within the vessel. Thus, droplets of the second phase are not carried to all parts of the tank, and a definite concentration profile for the dispersed phase exists within the two-phase region. The second type of inhomogeneity results from an unfavorable equilibrium between the dispersion and coalescence processes. While fluid-dynamic forces are again important, the dispersion and coalescence phenomena are much more complex and more strongly influenced by the properties of the liquids (i.e., density, viscosity, interfacial tension) than by the distribution of suspended phase within the emulsion.

A. Preliminary Considerations

If radial variations in concentration are small compared to the vertical (axial) variation, a relatively simple description of the dispersion in cylindrical agitators can be given. Figure 2 shows the range of possible distributions of the local volume=fraction $\emptyset_s$ as a function of the fractional tank height h, with the "origin" (h = 0) always taken at that end of the tank where the settled dispersible phase would lie.

Curve A in Fig. 2 represents complete inhomogeneity or "zero mixing," and has somewhat the physical appearance of a cross-section view through a

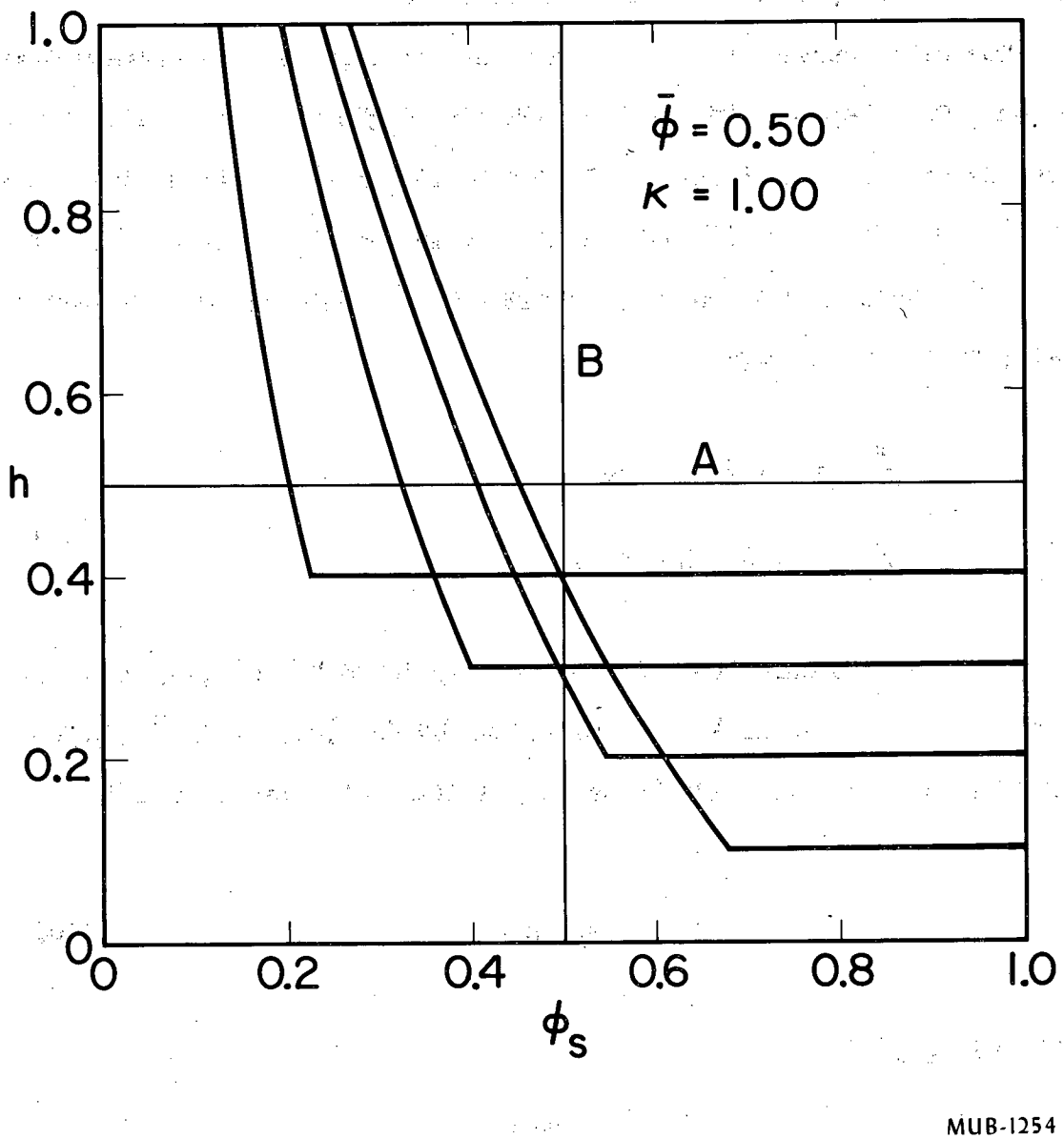

Fig. 2. Computed dispersed-phase distributions (exponential model).

stagnant agitator. Curve B represents the opposite extreme, or complete bulk homogeneity, for which a sample withdrawn from anywhere in the vessel would be identical in composition to the overall value $\overline{\phi}$.

The other curves in Fig. 2 represent one type of intermediate distribution. The shape of these curves and the height of the stagnant layer h_B, represented by the horizontal discontinuity in the profile, are somewhat arbitrary. The first restriction to satisfy is that the area to the left of (i.e., "under") each curve must be equal to $\overline{\phi}$. Because ϕ_s is independent of radial position, we have

$$\begin{aligned} \overline{\phi}_s &= f(h), \; h > h_B , \\ \phi_s &\geq 1.0 , \; h < h_B , \end{aligned} \tag{15}$$

where f(h) is a monotonic function such as expressed by Eq. (19) or (20), with the intermediate curves in Fig. 2 calculated by Eq. (20), with $\overline{\phi} = 0.50$, and $\kappa = 1.00$ throughout. In order to satisfy a material balance we have

$$\phi = \int_0^1 \phi_s \, dh , \tag{16}$$

or, from Eq. (15),

$$1\overline{\phi} = h_B + \int_{h_B}^{1.0} f(h) \, dh. \tag{17}$$

A further restriction on the functional form of f(h) arises from the coalescence process that is affecting the performance of the mixer. It is evident from physical considerations that a maximum upper limit exists for the

concentration ϕ_s of the dispersed phase; this limiting value is taken to be 0.70. In a situation of poor mixing, both a layer of "stagnant" second phase and a steep gradient for the ϕ_s distribution within the emulsion are likely to occur. The highest value for ϕ_s, ϕ_{max}, will occur at the interface, with any undispersed material at $h = h_B$, or otherwise at the end of the tank ($h = h_B = 0$). The ϕ_{max} restriction is most conveniently incorporated by transforming the variable h to the new form $h - h_B$, which can vary between zero and $(1 - h_B)$. The definition of f(h) in Eq. (15) can now be rewritten more explicitly (with the provision that $0 < \phi_{max} \leq 0.70$):

$$\frac{\phi_s}{\phi_{max}} = f(h - h_B) . \tag{18}$$

From the empirical viewpoint, the simplest explicit form for Eq. (18) would be the linear function

$$\frac{\phi_s}{\phi_{max}} = 1 - \kappa(h - h_B) ; \tag{19}$$

however, a more attractive theoretical basis exists for an exponential relation suggested by the Boltzmann distribution of molecules in a gravitational field:

$$\frac{\phi_s}{\phi_{max}} = e^{-\kappa(h - h_B)} \tag{20}$$

Our primary effort has been devoted to testing the exponential form, although the linear form remains an alternate empirical possibility.

The various parameters of Eq. (20) are illustrated in Fig. 3, where their relation to the physical system becomes more evident. (Fig. 3 also

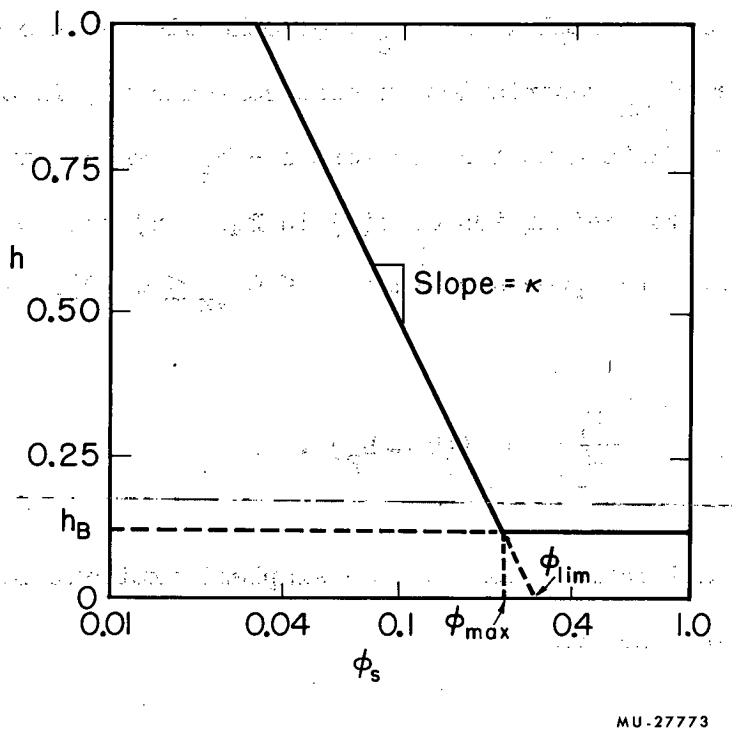

Fig. 3. The exponential distribution model (theoretical).

shows an extrapolated volume fraction, ϕ_{lim}, which is useful in calculating κ and h_B from experimental profiles of ϕ_s.)

The slope of the exponential distribution function κ becomes a valid measure of bulk homogeneity, varying from zero at perfect mixing to infinity at no mixing. A "theoretical mixing index," TMI, can then be defined as

$$\mathrm{TMI} = \frac{1}{1 + \kappa} . \tag{21}$$

This function has the familiar property of varying between 0 and 1, with 100 (TMI) being an analogous measure of "percent mixed."

The second paramenter in the model, h_B, is the height of the interface between the emulsion and the remaining dispersible (but undispersed) material. The value of h_B is therefore directly proportional to the volumn of "stagnant" material that is not participating in the mixing process.

B. Analysis for κ

If a true analogy to the statistical-mechanical model exits, κ may well depend upon the square of the ratio of local particle velocity V_s to the velocity of the continuous phase V_j that surrounds it. Thus we have

$$\kappa = f\left(\frac{V_s^{\,2}}{V_j^{\,2}}\right). \tag{22}$$

Let us consider a liquid mixture in an agitated tank, in the neighborhood of the impeller. The impeller acts to form a jet of relatively high-velocity fluid which diverges and causes circulation throughout the tank. As a

reasonable approximation, the liquid at the impeller tip can be considered to have a velocity proportional to the tip speed π NL. The local liquid velocity at any other point should then be related to the impeller velocity by the geometry of the agitator and the vessel.

For a turbine impeller, the area of the jet is proportional to LW. Because the jet velocity decreases with distance from the impeller, the local velocity should be inversely proportional to both tank height H and diameter T, or to the product TH in a simple cylindrical tank. Therefore, the average local velocity should be proportional to the impeller-tip speed and the ratio LW/TH (which we define as a geometrical group G), and we should have

$$V_j \propto (NL)\, G^x \quad . \tag{23}$$

Exponent x is included to allow for the expected nonlinear nature of the relationship.

The local particle velocity has been commonly characterized by a terminal settling velocity. For spheres falling in a laminar field, Stokes's equation is:

$$V_s = (\text{const}) \frac{g\, |\Delta \rho|\, d_p^2}{\mu_c} \quad . \tag{24}$$

Similarly, for conditions of isotropic turbulence, Newton's expression for terminal settling velocity is

$$V_s = (\text{const}) \left[\frac{g\, |\Delta \rho|\, d_p}{\rho_c} \right]^{1/2} \tag{25}$$

Considering a laminar-flow regime, substitution of Eqs. (23) and (24) Stokes's law into Eq. (22) yields

$$\kappa \propto \left[\frac{g\,|\Delta\rho|\,d_p^{\,2}}{\mu_c N L}\right]^2 \left(\frac{1}{G^{2x}}\right) . \qquad (26)$$

Upon rearrangement, this becomes

$$\kappa^{-1} \propto \left(\frac{N^2 L\,\rho_c}{g\,|\Delta\rho|}\right)^2 \left(\frac{N L^2\,\rho_c}{\mu_c}\right)^{-2} \left(\frac{L}{d_p}\right)^4 G^{2x} , \qquad (27)$$

or, in terms of the common names for the dimensionless groups, with $2x = y$,

$$\kappa^{-1} \propto (N_{Fr})^2 \; (N_{Re})^{-2} \; \left(\frac{L}{d_p}\right)^4 \; G^y . \qquad (28)$$

In a condition of isotropic turbulence, substitution of Newton's result (Eq. 25) into Eq. (22) similarly results in

$$\kappa^{-1} \propto N_{Fr} \left(\frac{L}{d_p}\right) G^y . \qquad (29)$$

In any real case of interest, the flow regime within the agitator will be neither laminar nor isotropically turbulent. However, when Eqs. (28) and (29) are examined, it will be seen that they can be combined into a single generic relationship of the form

$$\kappa^{-1} \propto (N_{Fr})^{2-2n} \; (N_{Re})^{-2+4n} \left(\frac{L}{d_p}\right)^{4-6n} G^y . \qquad (30)$$

Thus for the case of $n = \frac{1}{2}$, Eq. (30) reduces to Eq. (29), the result for isotropic turbulence. Similarly, for $n = 0$, Eq. (28) is obtained. Since neither isotropic turbulence nor laminar flow is encountered on the scale of the dispersed-particle diameters in an agitated tank, and since a dispersive process is in balance with a settling process, it would be possible in principle to find any value for n in this general region.

C. Analysis for h_B

The parameter h_B designates the height of a layer of second phase that remains undispersed after dybamic equilibrium is attained. Such a stagnant layer can occur as a result of two distinct types of behavior.

The first cause is inability of the emulsified phase to contain more dispersed phase, under the given agitation conditions, (i.e., a lack of "mixing power" in the agitation, which is a coalescence phenomenon). Under these conditions, the volume fraction of dispersed phase at the interface ϕ_{max} will have a limiting value of around 0.70. In this case, the entire homogeneity behavior can be described by the value of κ.

The second cause is inability of the main fluid motion to bring about dispersion of the residual liquid. In this case ϕ_{max} could have any value in the range $0 \leq \phi_{max} \leq 0.70$, as illustrated in Fig. 2. The remainder of this section discusses the factors affecting h_B in this case.

The dispersion process has been postulated to occur in three steps:

(a) an initial disturbance at the interface in the form of a wave,

(b) the formation of "ligaments" that break off from the wave crests,

(c) the continued breakup of these fragments into small droplets.

For the case of dispersion in an agitated vessel, the disturbing force is supplied by the jet of liquid circulating from the impeller. Once the dispersible phase has broken away from the bulk of remaining material into separate fragments, further size reduction becomes a process of droplet breakup in a turbulent field, as discussed previously.

Whenever fluid in an agitator remains undispersed, it is reasonable to assume that the interfacial disturbance, caused by the impeller jet, is too weak to propoagate unstable waves of large amplitude. The interfacial wave is then either stable or damped out, and no further "ligaments" are formed. For example, in a vessel with the impeller initially entirely within the continuous phase, as agitation commences and a portion of the second phase is dispersed, the dynamic interface evidently migrates toward the remote end of the vessel. Under some conditions, a point will be reached at which the relative velocity at the dynamic interface is insufficient to promote further dispersion. At this point, no further breakup occurs (in other words, equilibrium exists between the counter processes of dispersion and coalescence).

Many investigations have been made of wave behavior on a theoretical basis, as reported for example by Lamb,[26] and some of the more pertinent experimental work has been mentioned in the Introduction. The results of these investigations show that dispersion and coalescence phenomena can be described primarily in terms of the Reynolds, Weber, and Froude groups. These groups represent ratios of the strongest forces acting on the droplets:

$$\left.\begin{aligned} N_{Re} &= \frac{\text{Inertial force}}{\text{Viscous force}} \\ N_{We} &= \frac{\text{Inertial force}}{\text{Capillary force}} \\ N_{Fr} &= \frac{\text{Inertial force}}{\text{Gravitational force}} \end{aligned}\right\} . \qquad (31)$$

As discussed in regard to the functional relationships for κ, the inertial force is related to the impeller-tip velocity by the geometrical group, G = LW/TH. The physical properties of the emulsified portion are influenced by its composition and hence indirectly by $\overline{\phi}$. These considerations indicate that a likely functional form for h_B is

$$h_B = h_B (N_{Re}, N_{We}, N_{Fr}, G, \overline{\phi}) \tag{32}$$

D. Behavior of the Model Parameters

If the material balance (Eq. 17) is rewritten specifically for the exponential model (Eq. 20), the result is:

$$\overline{\phi} = h_B + \phi_{max} \int_{h_B}^{1} e^{-\kappa (h - h_B)} dh \tag{33}$$

Integration of (33) yields:

$$\overline{\phi} = h_B + \frac{\phi_{max}}{\kappa} \left\{ 1 - e^{-\kappa(1 - h_B)} \right\} . \tag{34}$$

For the situation where a large concentration gradient κ controls the presence of a nonzero h_B, Eq. (34) can be simplified by initially setting $h_B = 0$:

$$\overline{\phi} = \frac{\phi_{max}}{\kappa} \left[1 - e^{-\kappa} \right] . \tag{35}$$

As κ increases, at any $\overline{\phi}$, a value of κ will be reached for which $\phi_{max} = 0.70$. For any larger value of κ, since ϕ_{max} cannot exceed 0.70, h_B becomes nonzero and is determined from the material balance.

Upon substitution of $\phi_{max} = 0.70$ into Eq. (35) an iterative equation is obtained for determining this lower-limit value for κ, under "kappa-control" of the presence of an undispersed layer. The solution of this equation for a range of values for $\overline{\phi}$ was carried out on the IBM 650 computer. The results are shown in Fig. 4 with the regions of dispersion control and kappa (coalescence) control indicated.

The shape of the curve in Fig. 4 indicates that bulk homogeneity as a criterion for good mixing becomes increasingly important as the total volume-fraction of dispersed phase increases. For example, when $\overline{\phi} = 0.10$, a value κ as high as 7 (TMI = 13%) would still indicate mixing conditions limited by dispersion effects; whereas, at $\overline{\phi} = 0.50$, κ must be equal to 0.70 or less (TMI = 59%), for dispersion effects to control the presence of a stagnant layer.

In practice it will be exceedingly difficult to obtain mixing conditions where $\overline{\phi} > 0.60$. To obtain any value of $\overline{\phi} > 0.50$, care must be taken to locate the impeller within the phase that is intended to be continuous. Even then, phase inversion may occur in a continuous-flow system.

As a further indication of the effect of this coalescence limit upon mixing, curves of the exponential distribution function for various values of κ with $\overline{\phi} = 0.50$ and $\phi_{max} = 0.70$, are shown in Fig. 5. The steepest curve shows the limiting case, where $\kappa = 0.70$. The other curves illustrate the growth of h_B, as κ increases above the limiting value and more of the second phase coalesces. The curves cross each other as a consequence of the material balance.

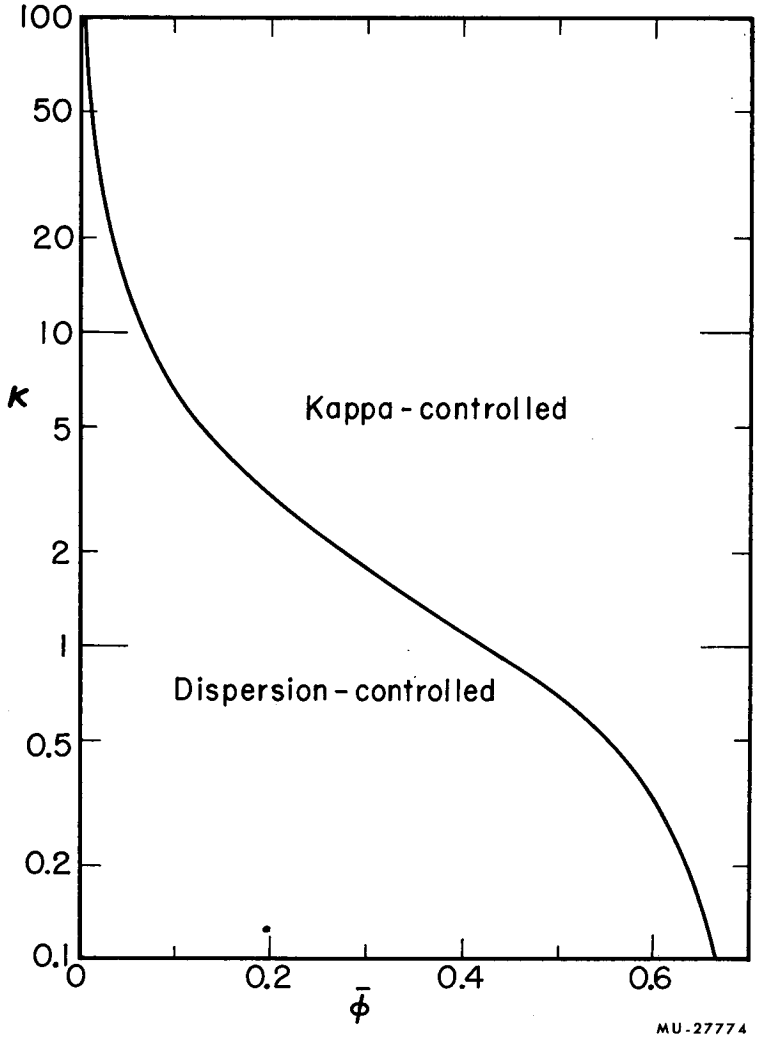

Fig. 4. Criterion for kappa control of h_B.

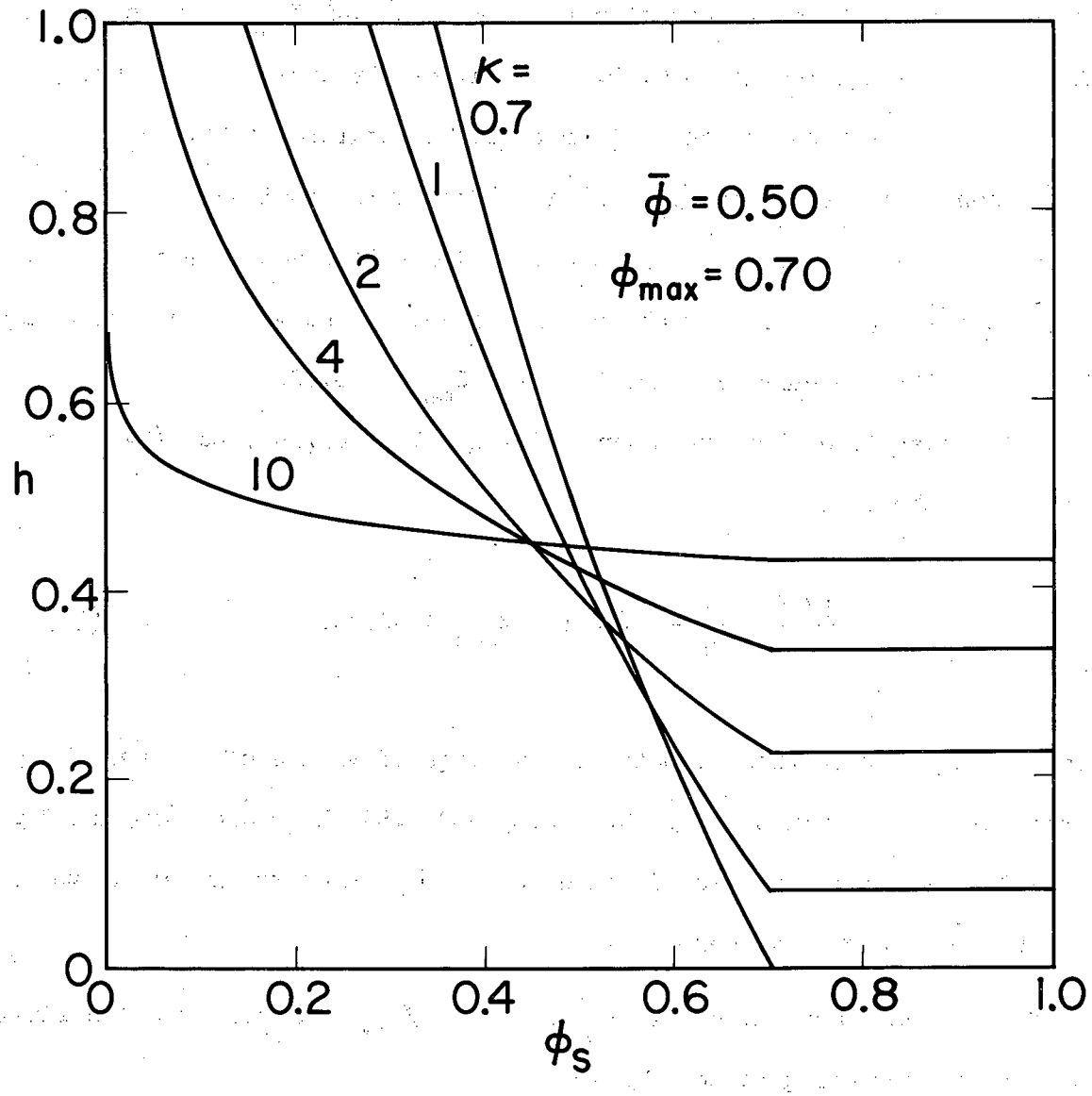

MUB-1255

Fig. 5. Computed dispersed-phase distributions with kappa-control.

The differences between the distributions of dispersed phase obtained under each of the two limitations of incomplete dispersion and incomplete uniformity may be noted by comparing Fig. 2 with Fig. 5. While h_B varies independently of κ in the former situation (Fig. 2) and ϕ_{max} ranges over a series of values all less than 0.70, the converse is true when a nonzero h_B arises from limitations of non-uniformity in the emulsion (Fig. 5).

When κ is below the minimum value for having coalescence control of h_B, a nonzero value for h_B may be obtained due to inadequate dispersive forces, as discussed in Sec. C above. These conditions will occur commonly in the region under the curve in Fig. 4, when $\phi_{max} < 0.70$.

In order to explore this type of incomplete mixing, Eq. (34) was rewritten in the form

$$\phi_{max} = \frac{(\overline{\phi} - h_B)\,\kappa}{1 - e^{-\kappa(1 - h_B)}}, \text{ with } \phi_{max} < 0.70. \tag{36}$$

Values of ϕ_{max} were then computed for a range of values of κ and h_B, for representative values of $\overline{\phi}$ (0.1, 0.3, and 0.5) which are shown in Figs. 6, 7, and 8 respectively. The dependence of ϕ_{max} upon the model parameters and upon $\overline{\phi}$ is shown by these curves:

(a) For any constant values of h_B and $\overline{\phi}$, ϕ_{max} increases to its limit of 0.70 with increasing values for κ.

(b) For any constant values of h_B and κ, ϕ_{max} increases with $\overline{\phi}$.

(c) For any constant values of $\overline{\phi}$ and κ, ϕ_{max} increases as h_B decreases.

(d) As κ decreases toward zero, ϕ_{max} approaches the asymptotic value, $\overline{\phi} - h_B$.

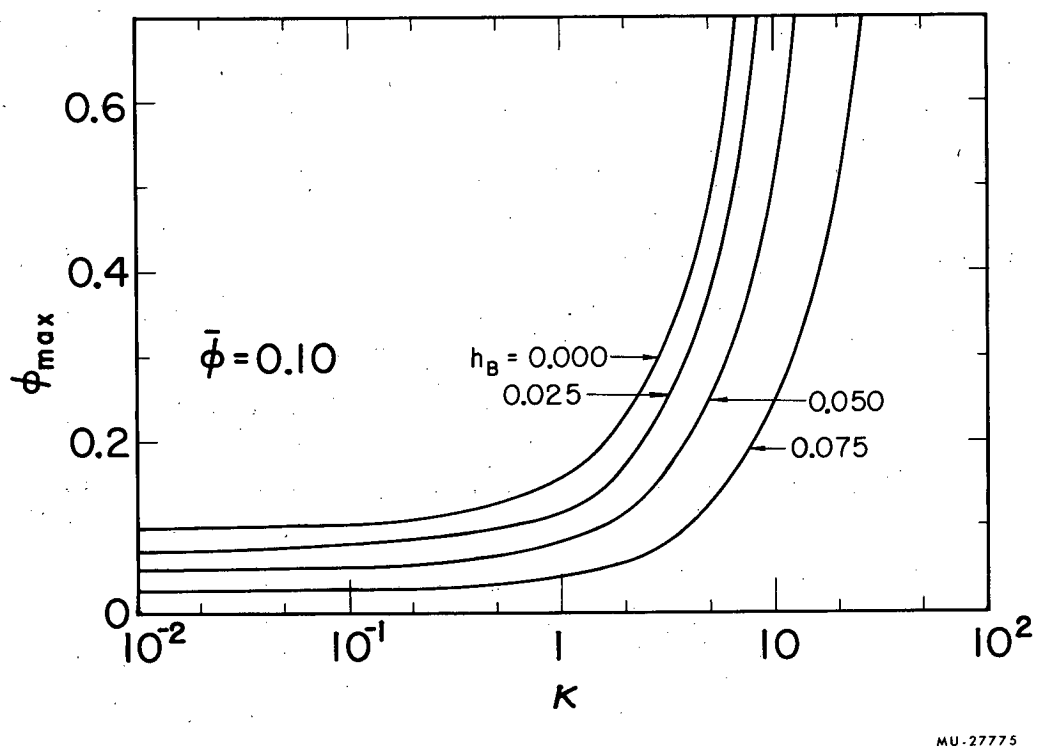

Fig. 6. Effect of κ and dispersion-controlled h_B upon ϕ_{max} ($\bar{\phi}$ = 0.10).

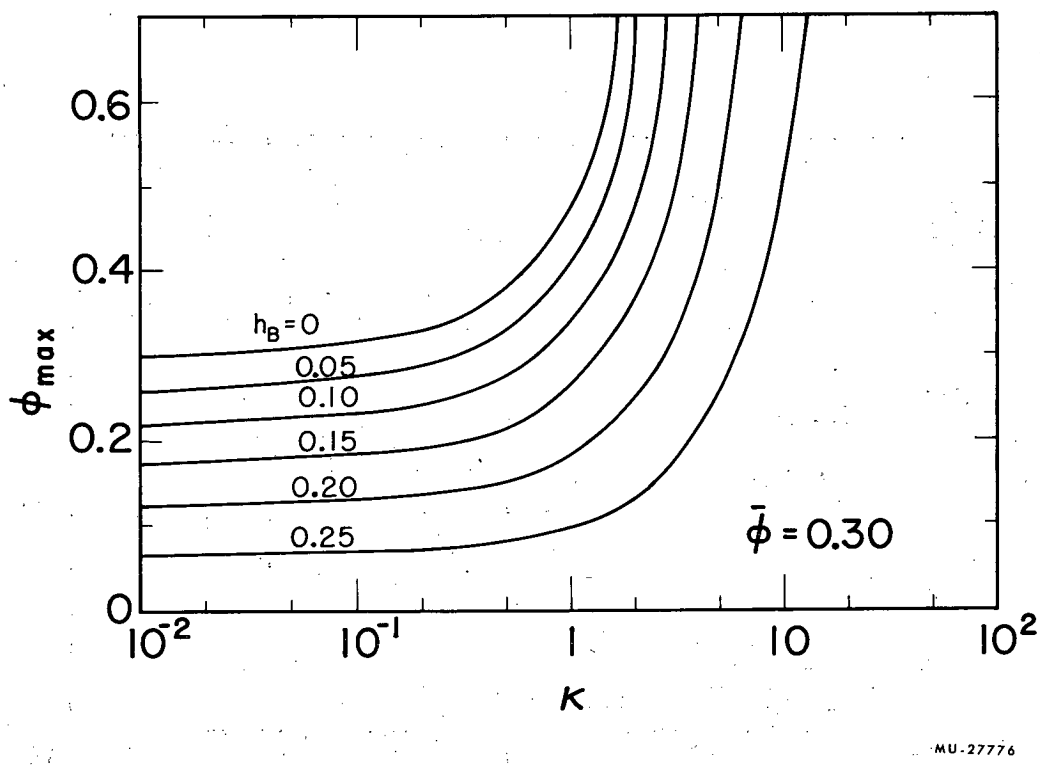

Fig. 7. Effect of κ and dispersion-controlled h_B upon ϕ_{max} ($\bar{\phi} = 0.30$).

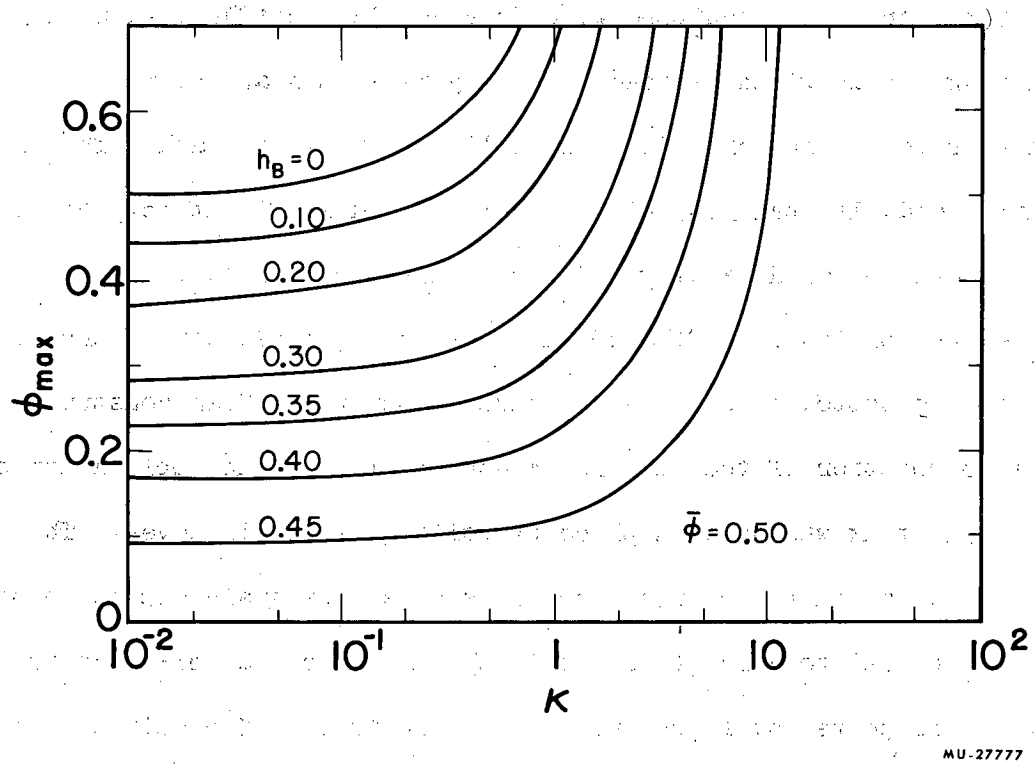

Fig. 8. Effect of κ and dispersion-controlled h_B upon ϕ_{max} ($\bar{\phi} = 0.50$).

IV. EXPERIMENTAL PROGRAM

A. Apparatus

The mixing vessels used in these studies were a cylindrical stainless steel tank 20-in. in height and diameter, and a smaller stainless steel tank (nominal 10-in.), also cylindrical, 8.87 in. high and 10.35 in. in diameter. The general configuration of the tanks in the assembled mounting is shown in Fig. 9. Both tanks were equipped with four vertical baffles, each one-tenth the tank diameter in width, spaced at 90 deg intervals around the tank wall and perpendicular to it, and extending the full height of the tank. The impellers were four-bladed flat paddles, with the blades and shaft entirely of stainless steel, and were centered axially and vertically for each run.

Because of its size, the 20-in. tank was equipped with a thrust-bearing assembly at the bottom to serve as a primary support. (This construction allowed free rotation of the tank for measuring the torque applied during separate studies.) The tank was held in place by bolting it to its cover. The cover, in turn, was attached to the frame by means of an integral-suspension ball-bearing unit welded to a length of steel channel; the channel-and-spindle assembly was supported by a post mounted on the frame. The entire cover assembly could be lifted clear of the tank to provide easy access for changing impellers and for cleaning, by sliding the post upward and fastening it with a spring-loaded stop.

The 10-in. tank used in preliminary work[2] was suspended from its cover by L-shaped bolts passed through holes in the ed ge of the cover and clamped under a lid at the top of the tank. The cover was attached to the frame in a manner similar to that used for the 20-in. cover.

For each tank, a cork gasket sealed the vessel to its cover, and a mercury seal between the cover and the impeller shaft assembly rendered the

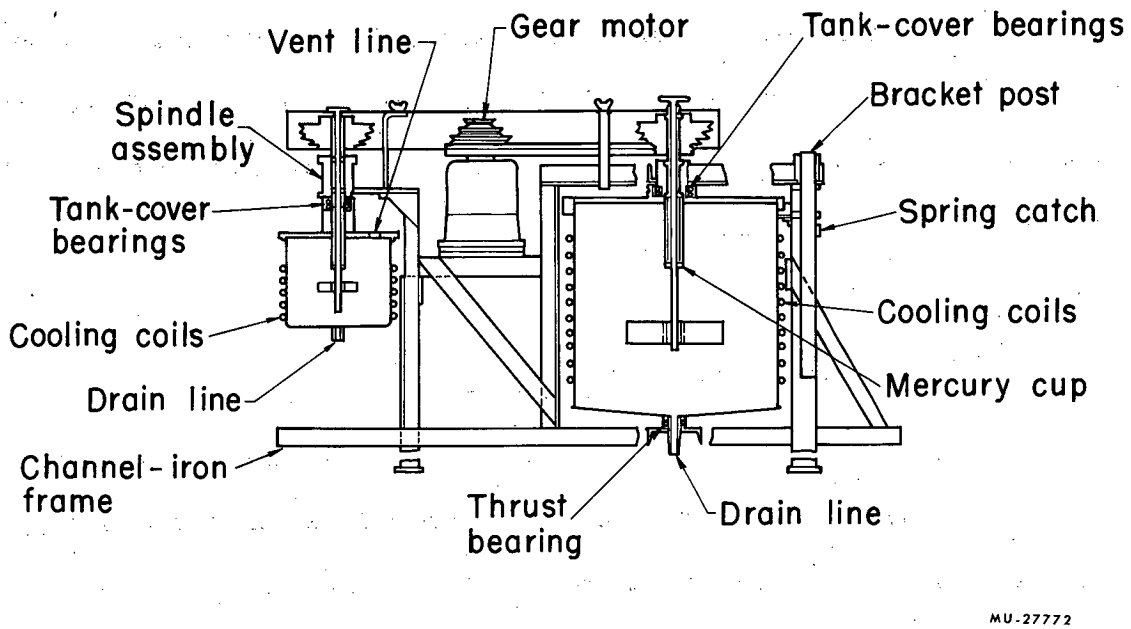

Fig. 9. Agitation apparatus.

assembled unit liquid- and air-tight. The cover had fittings for a thermometer well, a feed line, a vent, and sampling probes. A coil of $\frac{1}{4}$-in. o.d. copper tubing was soldered to the outside to allow circulation of cooling water for temperature control. A bottom drain was also provided.

The impellers for both tanks were driven by a V-belt drive connected to a 3/4-hp, 3-phase 60-cycle, 220-V, 216-rpm right-angle-gear motor supplied by Electra Motors, Inc. Step-cone pulleys were mounted on each of the impeller shafts and on the motor shaft, so that the impellers could be rotated at fixed speeds of 1.83, 2.83, 4.50 and 6.83 rps.

B. Sampling Probe

The probe used in this study was a length of stainless steel tubing of 3/16-in. o.d. by 1/32-in. i.d. The probe ended in a horizontal arm $5\frac{1}{2}$ in. long, and the inner diameter was tapered out to 1/16-in. at this end. The butt of an 18-ga hypodermic needle was soldered onto the upper end. The tube could be rotated and moved vertically through a packing gland that attached it to the tank cover. A Lucite handle was attached to the exterior part of the probe and aligned with the lower arm. A protractor was mounted on the tank cover and used with the Lucite handle to determine the radial position of the probe arm.

An array of sampling points was adopted initially, comprising five radial positions at each of six tank heights. It was assumed that angular symmetry about the tank axis would make measurements along more than one radius unnecessary; however, due to the nature of the sampling probe, the radial position of sampling varied through an angle of 48 deg around the axis of the vessel.

After the initial data were analyzed, it became apparent that radial fluctuations in concentration were negligible when compared with the distinct pattern of stratification. Consequently, the sampling array was revised to include more heights with fewer radial positions. The ultimate result was to draw samples from ten different heights but at only two radial locations. Since the phase of lower density was dispersed in nearly all the runs of this study, more of the samples were drawn from the upper half of the vessel, which was the section of greater interest The sampling arrays for this and for the preliminary investigation are shown in Figs. 10 and 11.

C. Materials and Physical Variables

The variables considered in this study were:

(1) Physical properties of the immiscible systems, i.e.,

(a) density (0.800 to 1.60 g/cm^3),

(b) viscosity (0.585 to 75.0 cP), and

(c) interfacial tension (12.0 to 48.0 dynes/cm).

(2) Mean volume-fraction of the dispersed phase (0.10 to 0.70).

(3) Impeller speed (1.83, 2.83, 4.50, 6.83 rps).

(4) Impeller and tank geometry (LW/TH ranging from 0.0256 to 0.122).

The physical properties of the liquids used in this investigation are listed in Table I. A compilation of all the geometrical systems studied appears in Table II.

In the kerosene-water runs, the dispersibility of the kerosene was found to decrease markedly after the mixture had remained in the tank for about four days. Upon inspection, a dark-colored material was observed in the static interface, resulting either from corrosion of the tank unit or from a catalytic

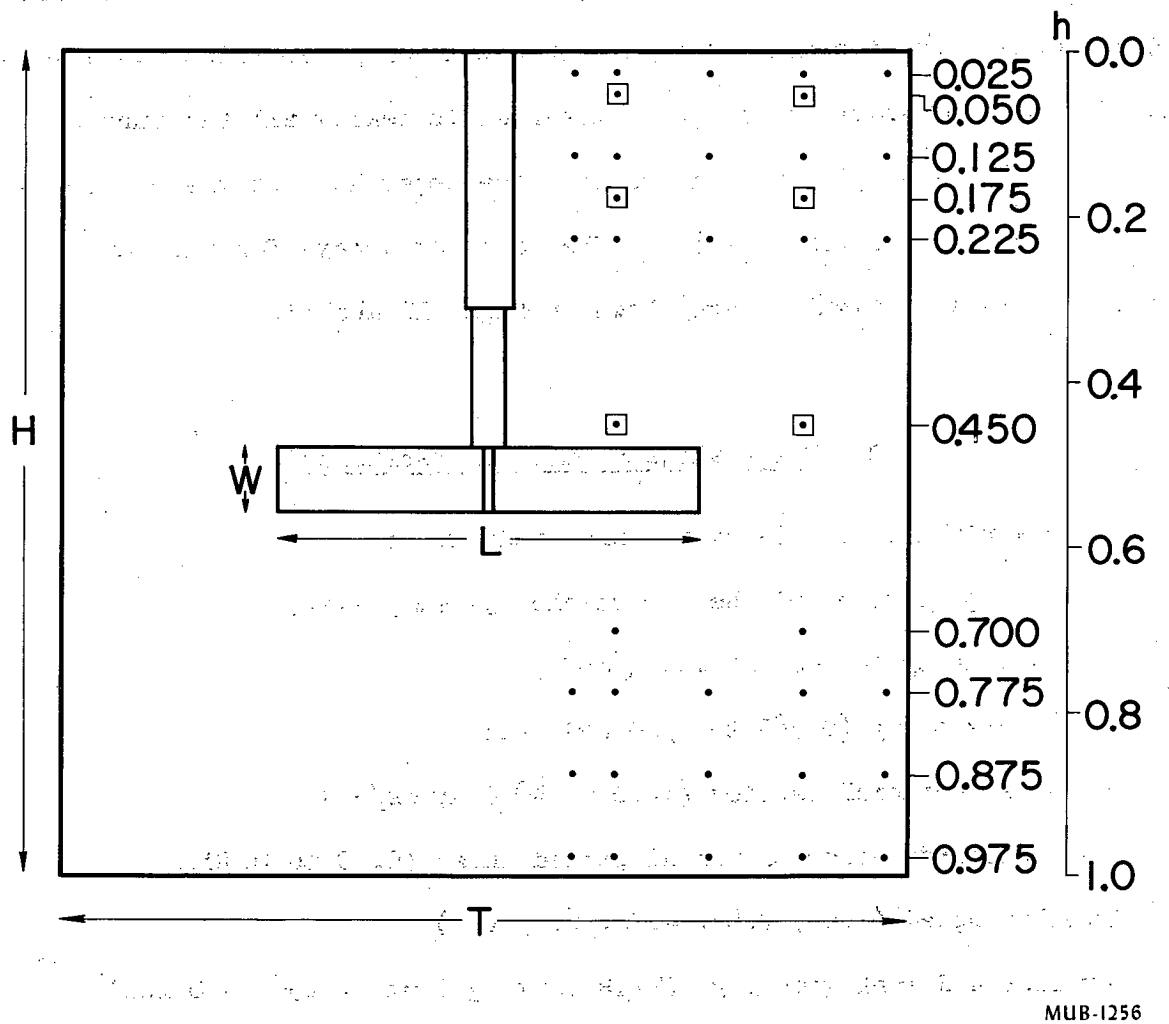

Fig. 10. Sampling-point array in agitator (side view).

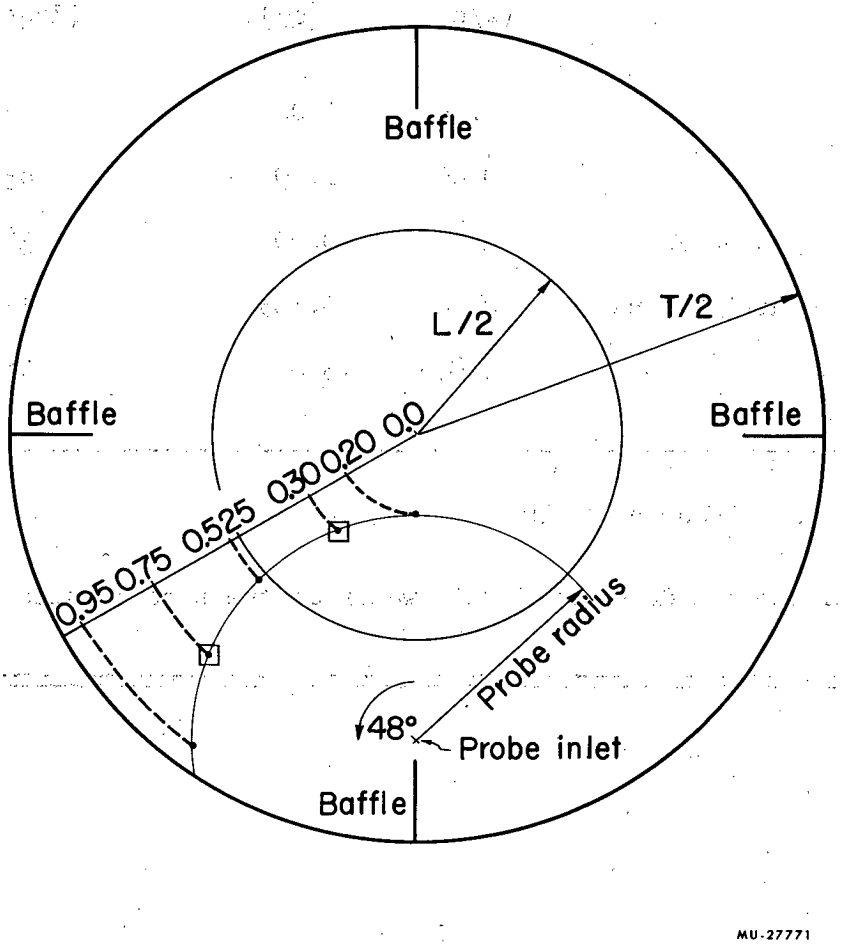

Fig. 11. Sampling-point array in agitator (top view).

Table I. Physical properties of liquids studied.[a]

Liquid	Density (g/cm^3)	Viscosity (cP)	Interfacial tension[b] (dynes/cm)
Water	0.998	1.00	----
Kerosene	0.803	2.69	43.6
Carbon tetrachloride	1.60	0.99	38.0
Methyl iso-butyl ketone	0.800	0.585	12.0
White oil	0.875	75.0	48.0

[a]All measurements made at 20°C.

[b]Interfacial tension determined with water as the second phase.

Table II. Dimensions of agitator geometries studied.[a]

Impeller length (in.)	Impeller width (in.)	Tank diameter (in.)	Tank height (in.)
2.50	0.94	10.35	8.87
5.00	0.94	10.35	8.87
7.50	0.94	10.35	8.87
6.77	1.65	10.35	8.87
5.00	2.00	20.0	20.0
6.67	2.00	20.0	20.0
10.00	2.00	20.0	20.0

[a]The baffles in the large tank were 2.0 in. wide. Those in the small tank were 1.0 in. wide.

decomposition of components in the kerosene. Consequently, the data reported on kerosene were all obtained with portions that had not been in the tank for more than 48 hours, during which time no deposits were evident. Before each refilling, the interior surfaces of the tank were rinsed with water and wiped clean.

D. Operating Procedure

At each mean volume-fraction, two complete sampling profiles were made for each impeller speed. One series was made while increasing the speed over the three steps listed, and another while decreasing the speed. The mixer was started at each speed and about fifteen minutes was allowed to reach equilibrium before sampling. This time proved to be ample. The samples were withdrawn from top to bottom in one series of measurements and from bottom to top in the other. The temperature of the tank contents was maintained at $20.0 \pm 0.5^{\circ}C$ by regulating the flow of cooling water.

Samples of 10 to 12 cm^3 were withdrawn with a hypodermic syringe, transferred to calibrated centrifuge cones, and centrifuged at 1200 rpm; then the level of the interface and the total volume were recorded for each sample. The sample was then returned to the tank in order to prevent the depletion of material, consequent air entrainment, and alteration of the mean volume-fraction.

In nearly all cases, the repeated measurements agreed with the original ones within 0.5 to 1.0% of total composition. Higher fluctuations were encountered when samples were withdrawn from points close to the dynamic phase boundary. Since these fluctuations were probably due to surface waves, an average of several measurements taken over a period of 15 to 30 minutes would seem to be representative for those points.

V. RESULTS AND DISCUSSION

A. Observed Distribution Profiles

The measured point-value volume-fractions, with their corresponding geometric variables, are compiled for each system of liquids tested (Tables IIIA-G incl.). In the two-phase region of the tank, the value of ϕ_s was found to be nearly constant in any plane parallel to the bottom of the vessel. Typical measurements along a radius of the tank at several fractional tank heights are shown in Fig. 12.

In the vertical direction, Fig. 13 shows that a concave-upward distribution pattern was observed, of the type predicted by Eq. (20) and illustrated in Fig. 2. This variation of concentration with height invalidates the assumption of symmetry about the impeller, proposed in an earlier study.[2]

The concept of dynamic equilibrium for the mixing operation, involving steady levels of concentration at various points, is confirmed by the results for numerous pairs of duplicate runs in Tables IIIA-G.

To test further the validity of the exponential-distribution model (Eq. 20), the data from Fig. 13 were replotted on semilog coordinates, as shown in Fig. 14. The linearity of the latter plot indicates that the theoretically attractive exponential model is also valid experimentally. The similarity between Figs. 3 and 14 should be noted.

B. Computational Methods and Results

After the exponential model had been adopted, a computer program was written for the IBM 650 to fit the "best values" of the parameters to the data for each run. The computational procedures employed are given in Appendix I and the results of the computation follow in Table V, also in the Appendix.

Table IIIA. Measured local volume-fraction ϕ_s for preliminary studies in 10-in. tank

Auxiliary data					Primary data[a]					
System	Agitator geometry L(in.)	Agitator geometry W(in.)	Speed N(rps)	$\overline{\phi}$	$\phi_{s,A}$	$\phi_{s,B}$	$\phi_{s,C}$	$\phi_{s,D}$	$\phi_{s,E}$	$\phi_{s,F}$
H_2O in	5.00	0.94	2.83	0.10	0.806	0.876	0.084	0.051	0.051	0.055
CCl_4	5.00	0.94	4.50	0.10	0.128	0.110	0.057	0.094	0.063	0.087
	5.00	0.94	2.83	0.20	1.000	1.000	0.363	0.658	0.041	0.035
	5.00	0.94	4.50	0.20	0.384	0.295	0.287	0.210	0.155	0.188
	5.00	0.94	4.50	0.40	0.465	0.429	0.475	0.424	0.339	0.361
	7.50	0.94	1.83	0.10	0.710	0.652	0.096	0.052	0.097	0.051
	7.50	0.94	1.83	0.20	1.000	1.000	0.260	0.435	0.106	0.089
	7.50	0.094	2.83	0.20	0.321	0.260	0.297	0.294	0.159	0.195
	7.50	0.94	2.83	0.40	0.429	0.405	0.431	0.405	0.385	0.376
	6.77	1.65	1.83	0.10	0.159	0.155	0.221	0.100	0.070	0.097
	6.77	1.65	1.83	0.10	0.159	0.155	0.221	0.100	0.070	0.097
	6.77	1.65	1.83	0.40	1.000	1.000	0.665	0.417	0.309	0.334
MIBK in H_2O	5.00	0.94	2.83	0.30	0.901	0.353	0.351	0.269	0.283	0.249
	5.00	0.94	2.83	0.50	0.980	0.565	0.622	0.532	0.488	0.512

Table IIIA. (Cont'd)

System	Auxiliary data: Agitator geometry L(in.)	W(in.)	Speed N(rps)	$\bar{\phi}$	Primary data[a]: $\phi_{s,A}$	$\phi_{s,B}$	$\phi_{s,C}$	$\phi_{s,D}$	$\phi_{s,E}$	$\phi_{s,F}$
H_2O in MIBK[b]	5.00	0.94	2.83	0.30	0.241	0.281	0.213	0.266	0.471	0.360

[a]Locations (see also Figs. 10 and 11):

Letter	h	r
A	0.05	0.30
B	0.05	0.75
C	0.25	0.30
D	0.25	0.75
E	0.45	0.30
F	0.45	0.75

[b]Since the denser phase is dispersed the sampling locations are:

Letter	h	r
A	0.95	0.30
B	0.95	0.75
C	0.75	0.30
D	0.75	0.75
E	0.55	0.30
F	0.55	0.75

Table IIIB. Measured local volume-fraction ϕ_s for preliminary studies in 20-in. tank.

Auxiliary data					Primary data[a]					
System	Agitator geometry L(in.)	Agitator geometry W(in.)	Speed N(rps)	$\bar{\phi}$	$\phi_{s,A}$	$\phi_{s,B}$	$\phi_{s,C}$	$\phi_{s,D}$	$\phi_{s,E}$	$\phi_{s,F}$
White oil in H_2O	5.00	2.00	6.83	0.20	0.207 0.217	0.199 0.238	0.204 0.204	0.208 0.200	0.203 0.207	0.211 0.212
	5.00	2.00	4.50	0.40	0.700 0.580	0.408 0.464	0.477 0.514	0.380 0.376	0.477 0.423	0.391 0.398
	5.00	2.00	6.83	0.40	0.458 0.438	0.414 0.411	0.430 0.432	0.380 0.403	0.413 0.426	0.395 0.400
	5.00	2.00	6.83	0.60	0.658 0.659	0.622 0.615	0.628 0.640	0.584 0.579	0.616 0.610	0.592 0.580
	10.00	2.00	1.83	0.20	0.234 0.237	0.207 0.210	0.236 0.250	0.206 0.193	0.230 0.227	0.207 0.214
	10.00	2.00	2.83	0.20	0.220 0.224	0.207 0.219	0.227 0.232	0.216 0.200	0.224 0.222	0.210 0.204
	10.00	2.00	1.83	0.40	0.732 0.553	0.453 0.446	0.471 0.463	0.413 0.383	0.440 0.441	0.392 0.404
	10.00	2.00	2.83	0.40	0.436 0.436	0.406 0.410	0.436 0.438	0.378 0.392	0.426 0.411	0.399 0.416
	10.00	2.00	1.83	0.60	0.668 0.638	0.587 0.595	0.629 0.668	0.559 0.575	0.677 0.604	0.569 0.586
	10.00	2.00	2.83	0.60	0.631 0.627	0.604 0.593	0.631 0.631	0.558 0.559	0.619 0.587	0.556 0.574

Table IIIB. (Cont'd)

System	Auxiliary data: Agitator geometry L(in.)	W(in.)	Speed N(rps)	$\bar{\phi}$	Primary data[a]: $\phi_{s,A}$	$\phi_{s,B}$	$\phi_{s,C}$	$\phi_{s,D}$	$\phi_{s,E}$	$\phi_{s,F}$
H_2O white oil[b]	5.00	2.00	4.50	0.20	0.124 0.136	0.113 0.104	0.139 0.126	0.134 0.114	0.147 0.124	0.136 0.123
	10.00	2.00	1.83	0.20	0.189 0.191	0.187 0.174	0.187 0.189	0.200 0.159	0.188 0.184	0.185 0.181
	10.00	2.00	2.83	0.20	0.200 0.188	0.197 0.184	0.189 0.187	0.142 0.159	0.170 0.175	0.155 0.164
	10.00	2.00	4.50	0.20	0.178 0.183	0.180 0.194	0.185 0.185	0.160 0.152	0.179 0.175	0.154 0.160

[a]Locations (see also Figs. 10 and 11):

Letter	h	r
A	0.05	0.30
B	0.05	0.75
C	0.25	0.30
D	0.25	0.75
E	0.45	0.30
F	0.45	0.75

[b]Since the more dense phase is dispersed the sampling locations are:

Letter	h	r
A	0.95	0.30
B	0.95	0.75
C	0.75	0.30
D	0.75	0.75
E	0.55	0.30
F	0.55	0.75

Table IIIC. Measured local volume-fractions $\emptyset_s$ for detailed studies in 20-in. tank (kerosene in H_2O; $\bar{\emptyset}$ = 0.10, L = 6.67 in., W = 2.00 in.).

h \ r	0.30	0.30	0.475	0.475	0.75	0.75	0.95	0.95
(A) N = 1.83 rps								
0.025	0.992	0.992	1.000	1.000	1.000	1.000	1.000	1.000
0.050	1.000	1.000			0.994	0.992		
0.125	0.472	0.385	0.296	0.315	0.188	0.170	0.131	0.180
0.175	0.434	0.775			0.224	0.149		
0.225	0.000	0.000	0.000	0.000	0.000	0.000	0.000	0.000
0.450	0.000	0.000			0.000	0.000		
0.700	0.000	0.000			0.000	0.000		
0.775	0.000	0.000	0.000	0.000	0.000	0.000	0.000	0.000
0.875	0.000	0.000	0.000	0.000	0.000	0.000	0.000	0.000
0.975	0.000	0.000	0.000	0.000	0.000	0.000	0.000	0.000
(B) N = 2.83 rps								
0.025	0.984	0.991	1.000	0.996	1.000	1.000	1.000	1.000
0.050	0.974	0.976			0.984	0.958		
0.125	0.121	0.058	0.059	0.043	0.053	0.035	0.052	0.035
0.175	0.155	0.175			0.054	0.059		
0.225	0.156	0.036	0.034	0.028	0.050	0.055	0.042	0.028
0.450	0.025	0.046			0.035	0.027		
0.700	0.026	0.028			0.029	0.034		
0.775	0.035	0.019	0.027	0.018	0.034	0.027	0.044	0.027
0.875	0.025	0.036	0.026	0.028	0.043	0.035	0.027	0.028
0.975	0.026	0.026	0.026	0.026	0.026	0.027	0.027	0.027

Table IIIC. (Cont'd)

(C) N = 4.50 rps

h \ r	0.30	0.30	0.475	0.475	0.75	0.75	0.95	0.95
0.025	0.113	0.110	0.107	0.107	0.054	0.108	0.109	0.100
0.050	0.103	0.105			0.101	0.064		
0.125	0.096	0.104	0.096	0.117	0.100	0.110	0.103	0.108
0.175	0.107	0.115			0.101	0.105		
0.225	0.071	0.115	0.096	0.107	0.100	0.164	0.095	0.105
0.450	0.064	0.108			0.147	0.059		
0.700	0.092	0.089			0.099	0.092		
0.775	0.089	0.108	0.097	0.106	0.089	0.103	0.089	0.083
0.875	0.106	0.105	0.096	0.108	0.103	0.109	0.096	0.106
0.975	0.111	0.097	0.105	0.103	0.105	0.106	0.108	0.080

Table IIID. Measured local volume-fractions $\emptyset_s$ for detailed studies in 20-in. tank (kerosene in H_2O; $\bar{\emptyset} = 0.20$, $L \cong 6.67$ in., $W = 2.00$ in.).

(D) N = 1.83 rps								
h \ r	0.30	0.30	0.475	0.475	0.75	0.75	0.95	0.95
0.025	0.996	0.991	1.000	1.000	1.000	1.000	1.000	1.000
0.050	1.000	1.000			1.000	1.000		
0.125	1.000	1.000	1.000	1.000	1.000	1.000	1.000	1.000
0.175	1.000	1.000			1.000	1.000		
0.225	0.777	0.860	0.861	0.264	0.575	0.259	0.315	0.018
0.450	0.018	0.000			0.000	0.000		
0.700	0.000	0.000			0.000	0.000		
0.775	0.000	0.000	0.000	0.000	0.000	0.000	0.000	0.000
0.875	0.000	0.000	0.000	0.000	0.000	0.000	0.000	0.000
0.975	0.000	0.000	0.000	01000	0.000	0.000	0.000	0.000
(E) N = 2.83 rps								
0.025	0.992	1.000	1.000	1.000	1.000	1.000	1.000	1.000
0.050	0.997	0.998			0.992	0.995		
0.125	0.950	0.874	0.959	0.814	0.822	0.808	0.807	0.824
0.175	0.433	0.915			0.172	0.903		
0.225	0.081	0.109	0.143	0.109	0.096	0.107	0.088	0.091
0.450	0.103	0.072			0.077	0.083		
0.700	0.078	0.069			0.078	0.084		
0.775	0.071	0.061	0.071	0.068	0.066	0.083	0.073	0.067
0.875	0.071	0.078	0.063	0.063	0.071	0.084	0.062	0.087
0.975	0.054	0.055	0.062	0.070	0.082	0.060	0.063	0.092

Table IIID. (Cont'd)

(F) N = 4.50 rps

h \ r	0.30	0.30	0.475	0.475	0.75	0.75	0.95	0.95
0.025	0.239	0.232	0.243	0.239	0.217	0.213	0.202	0.231
0.050	0.211	0.215			0.223	0.216		
0.125	0.211	0.211	0.202	0.205	0.202	0.209	0.200	0.202
0.175	0.211	0.211			0.214	0.205		
0.225	0.207	0.222	0.209	0.216	0.204	0.219	0.212	0.213
0.450	0.218	0.209			0.170	0.205		
0.700	0.195	0.208			0.207	0.196		
0.775	0.198	0.210	0.198	0.200	0.200	0.207	0.152	0.211
0.875	0.188	0.212	0.202	0.204	0.211	0.216	0.207	01205
0.975	0.207	0.198	0.212	0.198	0.200	0.204	0.205	0.195

Table IIIE. Measured local volume-fractions $\emptyset_s$ for detailed studies in 20-in. tank (kerosene in H_2O; $\emptyset = 0.40$, L = 6.67 in., W = 2.00 in.).

h \ r	0.20	0.20	0.30	0.30	0.475	0.475	0.75	0.75	0.95	0.95
(G) N = 2.83 rps										
0.025	1.000	1.000	1.000	1.000	1.000	1.000	1.000	0.974	1.000	0.978
0.050			0.677	0.994			0.991	1.000		
0.125	0.530	0.600	0.469	0.393	0.477	0.407	0.414	0.353	0.411	0.379
0.175			0.385	0.402			0.393	0.377		
0.225	0.413	0.438	0.365	0.471	0.371	0.351	0.393	0.381	0.357	0.377
0.450			0.381	0.391			0.374	0.345		
0.700			0.355	0.363			0.362	0.332		
0.775	0.372	0.357	0.345	0.345	0.361	0.363	0.368	0.360	0.377	0.365
0.875	0.333	0.327	0.342	0.357	0.359	0.363	0.367	0.362	0.371	0.375
0.975	0.287	0.274	0.312	0.320	0.366	0.343	0.355	0.364	0.381	0.374
(H) N = 4.50 rps										
0.025		0.563	0.440	0.389	0.431	0.432	0.422	0.434	0.431	0.414
0.050			0.407				0.409			
0.125	0.403	0.422	0.385	0.391	0.423	0.407	0.419	0.383	0.420	0.407
0.175			0.407				0.407			
0.225	0.419	0.371	0.410	0.416	0.373	0.419	0.419	0.407	0.397	0.377
0.450			0.396				0.393			
0.700			0.393				0.402			
0.775	0.402	0.405	0.407	0.409	0.414	0.413	0.420	0.422	0.418	0.410
0.875	0.430	0.450	0.381	0.402	0.409	0.414	0.421	0.430	0.416	0.405
0.975	0.403	0.395	0.405	0.402	0.412	0.420	0.417	0.404	0.419	0.417

Table IIIF. Measured local volume fractions $\emptyset_s$ for detailed studies in 20-in. tank (kerosene in H_2O; $\overline{\emptyset}$ = 0.40, L = 6.67 in., W = 2.00 in.).

(I) N = 1.83 rps

h \ r	0.20	0.20	0.20	0.30	0.30	0.30	0.475	0.475
0.025	1.000	1.000	1.000	1.000	1.000	1.000	1.000	1.000
0.050				1.000	1.000			
0.125	1.000	1.000	1.000	1.000	1.000	1.000	1.000	1.000
0.175				1.000	1.000			
0.225	1.000	1.000	1.000	1.000	1.000	1.000	1.000	1.000
0.450				0.426	0.392			
0.700				0.009	0.009			
0.775	0.033	0.027	0.010	0.034	0.034	0.027	0.034	0.033
0.875	0.016	0.025	0.010	0.027	0.033	0.019	0.016	0.034
0.975	0.016	0.033	0.019	0.023	0.025	0.018	0.015	0.024

h \ r	0.475	0.75	0.75	0.75	0.95	0.95	0.95
0.025	1.000	1.000	1.000	1.000	1.000	1.000	1.000
0.050		0.992	0.992				
0.125	1.000	1.000	1.000	1.000	1.000	1.000	1.000
0.175		1.000	1.000				
0.225	1.000	1.000	1.000	1.000	1.000	1.000	1.000
0.450		0.017	0.034				
0.700		0.009	0.009				
0.775	0.018	0.025	0.025	0.027	0.033	0.050	0.020
0.875	0.009	0.025	0.034	0.017	0.025	0.034	0.028
0.975	0.018	0.016	0.031	0.009	0.024	0.031	0.009

Table IIIG. Measured local volume fractions $\overline{\phi}_s$ for detailed studies in 20-in. tank (kerosene in H_2O)

	(J)	(K)	(L)		(M)	(N)	(O)	(P)	(Q)	(R)
$\overline{\phi}$	0.40	0.40	0.21		0.21	0.12	0.12	0.12	0.40	0.40
N(rsp)	1.83	2.83	1.83		2.83	1.83	4.50	6.83	2.83	4.50
L(in.)	10.00	10.00	10.00		10.00	10.00	5.00	5.00	5.00	5.00
W(in.)	2.00	2.00	2.00		2.00	2.00	2.00	2.00	2.00	2.00
$\phi_{s,1}$[a]	0.661	—	0.573	0.710	0.241	0.407	0.991	0.127	1.000	0.992
$\phi_{s,2}$	0.824	0.395	0.421	0.650	0.235	0.280	1.000	0.122	1.000	1.000
$\phi_{s,3}$	0.496	0.409	0.407	0.333	0.218	0.167	0.988	0.120	1.000	1.000
$\phi_{s,4}$	0.418	0.395	0.234	0.246	0.218	0.110	0.086	0.121	1.000	1.000
$\phi_{s,5}$	0.403	0.410	0.230	0.256	0.231	0.149	0.303	0.124	1.000	1.000
$\phi_{s,6}$	0.413	0.400	0.235	0.222	0.223	0.126	0.048	0.116	1.000	1.000
$\phi_{s,7}$	0.417	0.400	0.243	0.190	0.222	0.128	0.033	0.116	1.000	1.000
$\phi_{s,8}$	0.397	0.392	0.220	0.217	0.211	0.124	0.025	0.116	1.000	1.000
$\phi_{s,9}$	0.402	0.397	0.231	0.225	0.217	0.151	0.016	0.123	1.000	1.000
$\phi_{s,10}$	0.418	0.403	0.212	0.222	0.214	0.120	0.016	0.110	1.000	1.000
$\phi_{s,11}$	0.404	0.432	0.200	0.209	0.217	0.109	0.025	0.107	0.653	0.231
$\phi_{s,12}$	0.391	0.398	0.200	0.200	0.207	0.107	0.025	0.113	0.033	0.175
$\phi_{s,13}$	0.387	0.393	0.183	0.179	0.164	0.082	0.018	0.103	0.008	0.134
$\phi_{s,14}$	0.377	0.400	0.184	0.192	0.212	0.092	0.017	0.112	0.025	0.169
$\phi_{s,15}$	0.376	0.379	0.180	0.158	0.254	0.087	0.017	0.107	0.017	0.161
$\phi_{s,16}$	0.344	0.393	0.179	0.182	0.205	0.106	0.017	0.160	0.018	0.171
$\phi_{s,17}$	0.375	0.384	0.161	0.167	0.213	0.074	0.018	0.111	0.008	0.150
$\phi_{s,18}$	0.350	0.397	0.207	0.205	0.210	0.104	0.025	0.115	0.004	0.181

Table IIIG (Cont'd)

	(J)	(K)	(L)		(M)	(N)	(O)	(P)	(Q)	(R)
$\phi_{s,18}$	0.350	0.397	0.207	0.205	0.210	0.104	0.025	0.115	0.004	0.181
$\phi_{s,19}$	0.374	0.377	0.151	0.153	0.203	0.076	0.009	0.115	0.008	0.129
$\phi_{s,20}$	0.328	0.380	0.171	0.179	0.210	0.088	0.017	0.109	0.017	0.159

[a] Sampling locations (see also Figs. 10 and 11):

h \ r	0.30	0.75	h \ r	0.30	0.75	h \ r	0.30	0.75
0.025	1	2	0.225	9	10	0.875	17	18
0.050	3	4	0.450	11	12	0.975	19	20
0.124	5	6	0.700	13	14			
0.175	7	8	0.775	15	16			

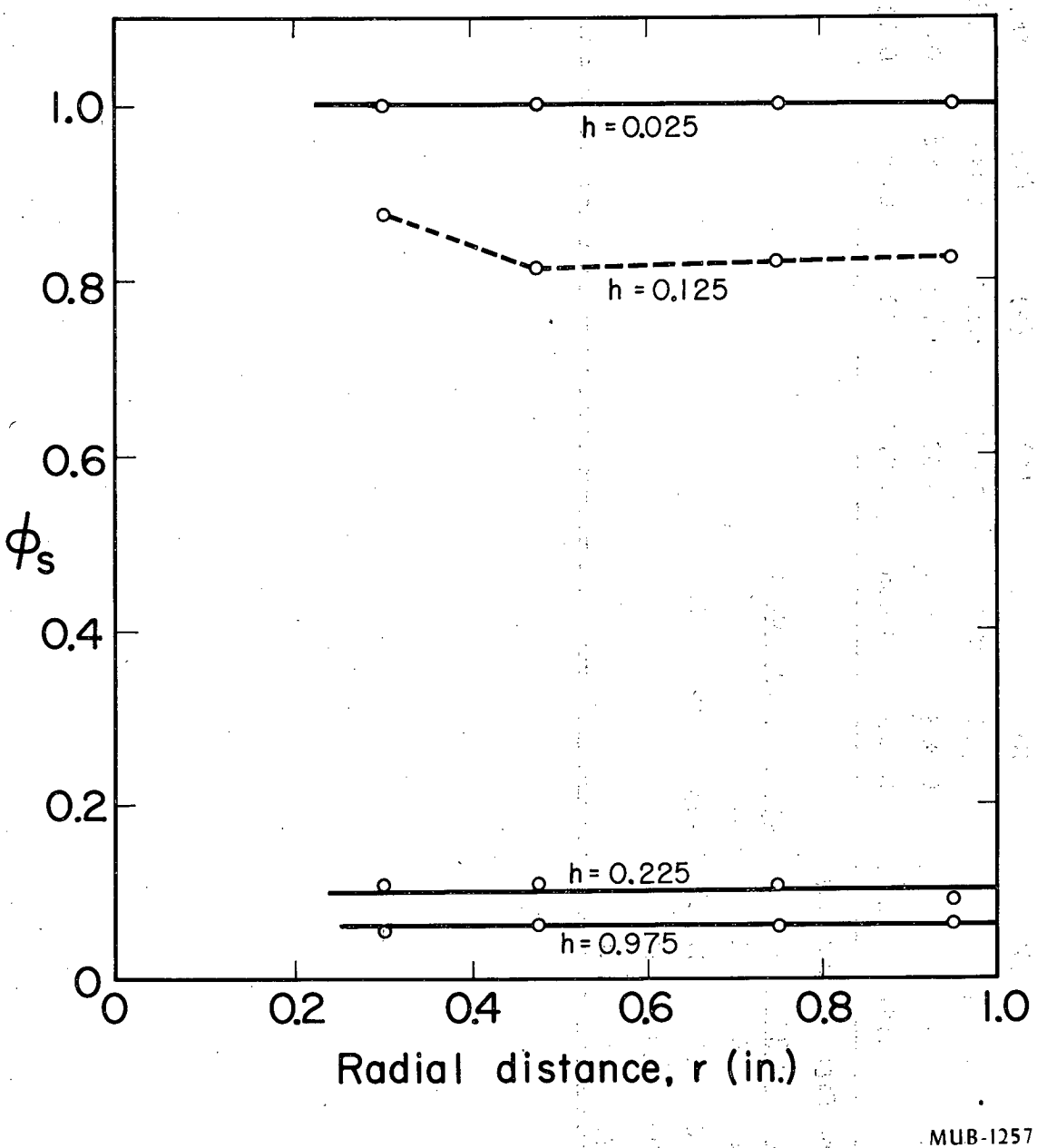

Fig. 12. Observed dispersed-phase volume fraction vs radial position.

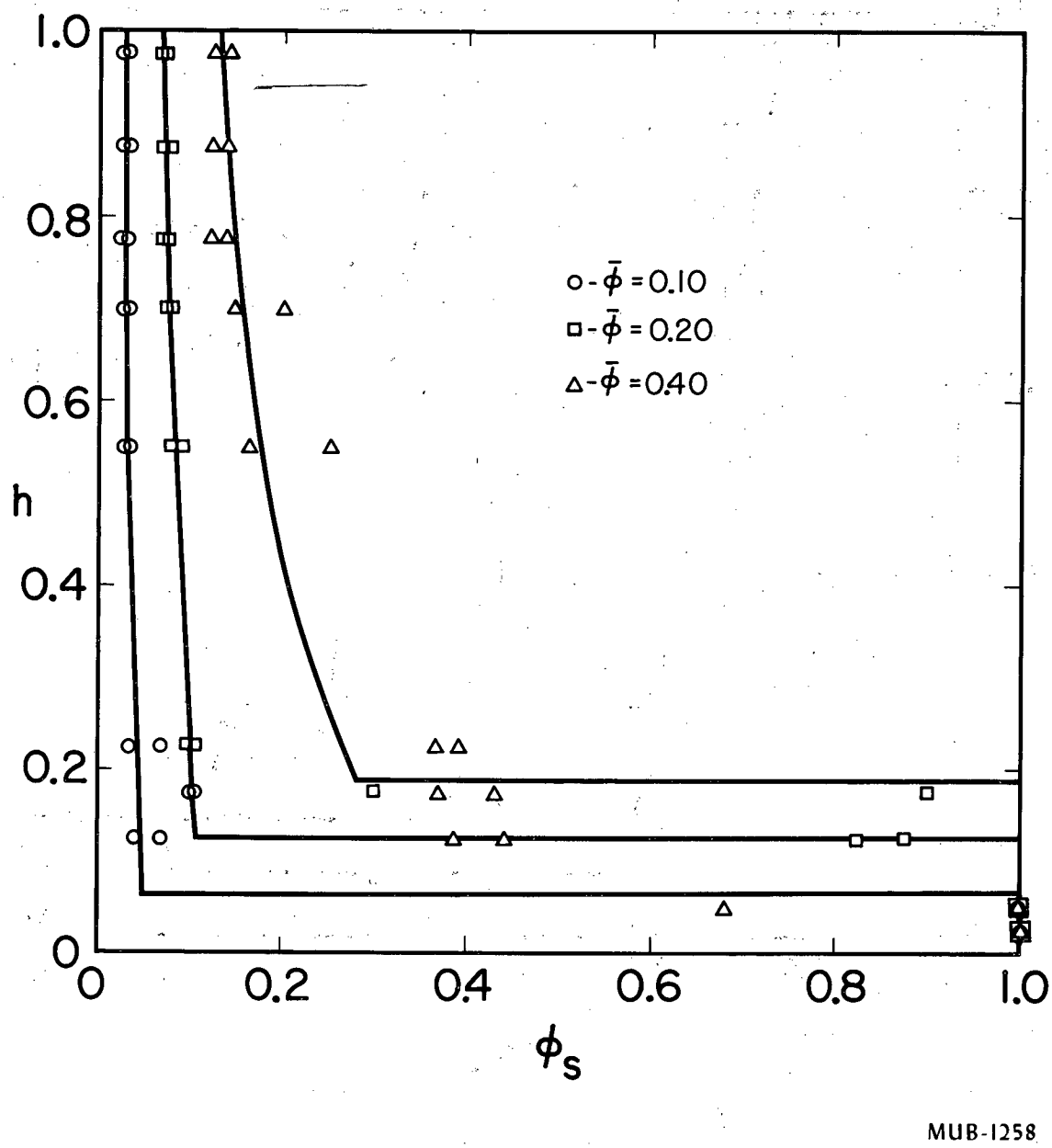

Fig. 13. Observed dispersed-phase distributions.

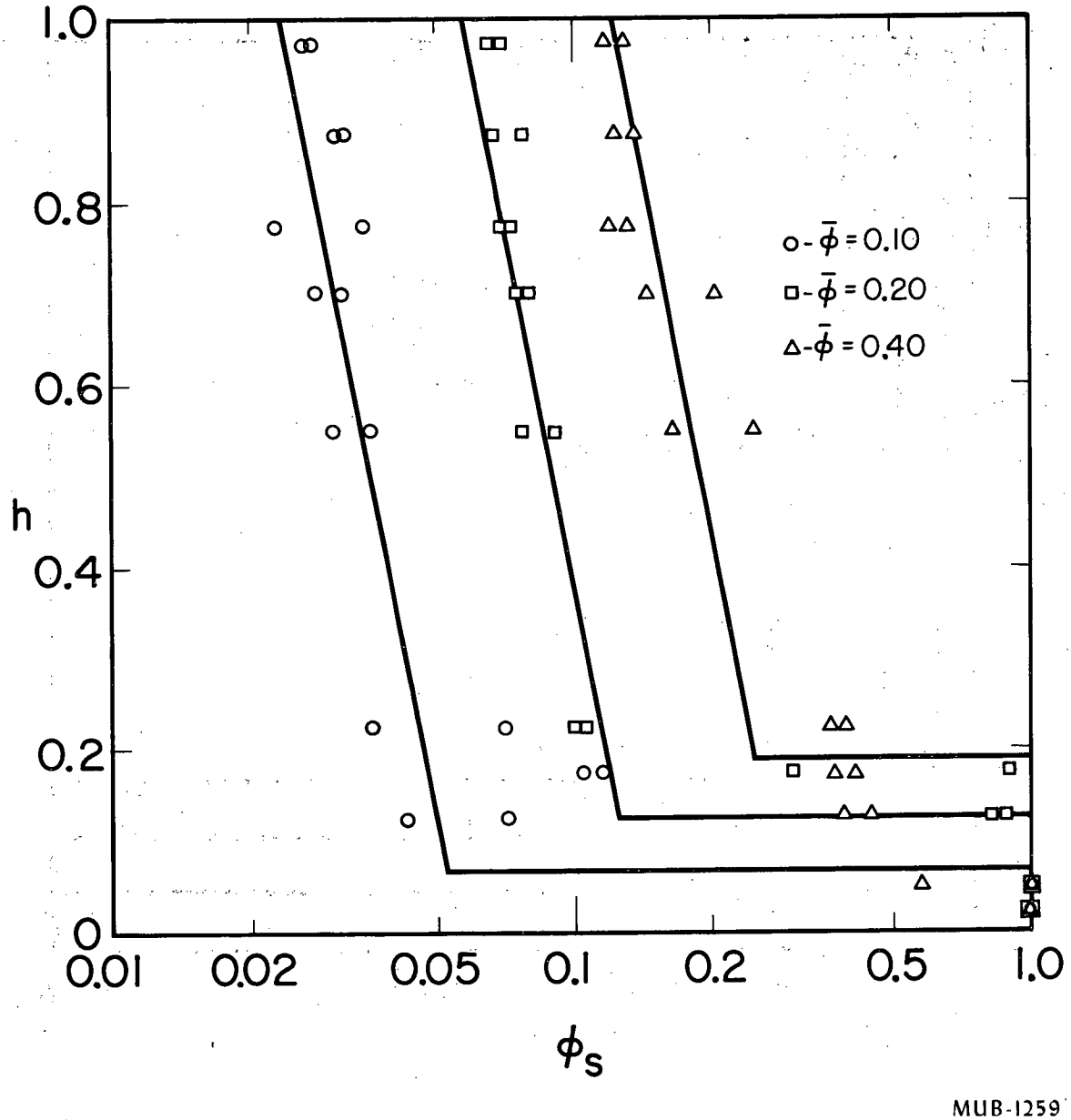

Fig. 14. Observed distribution of the dispersed phase, on semilog coordinates.

As a further check of the quality of fit of the exponential model, $\emptyset_s$ values were computed at the same values for h at which experimental measurements had been made. To facilitate a comparison between the observed and these smoothed fit values, EMI was calculated for both sets of data for each run. The details of these calculations will also be found in the appendix.

The effectiveness of the exponential model as a representation of the data is shown by the excellent correlation between the observed and smoothed-fit values of EMI in Fig. 15.

It should be emphasized that the excellent agreement between predicated and observed values of EMI is a standard for accepting Eq. (20) only as a reasonable representation of the dispersed-phase distribution. That EMI, or any other single parameter, is inadequate to describe this distribution can be illustrated by Fig. 16, which compares the two single criteria, EMI and TMI. As this figure shows, the two measures are very poorly correlated. Although TMI reliably indicates the approach to bulk homogeneity in the two-phase region of the vessel, it does not contain an explicit provision for evaluating the volume of (dispersible) undispersed phase remaining. However, the definition of EMI (Eqs. 11 and 12) does implicitly contain both of the requirements for homogeneity $\kappa = 0$ and $h_B = 0$. It is evident from Fig. 16 that EMI is too insensitive to the individual parameters to be an accurate and useful standard.

As shown in the Appendix, the dimensionless groups to be used in subsequent correlations were calculated for each run. The equations used for mixture properties have evolved from previous studies at this laboratory[2,22] and are believed to be the most reliable now available. The average drop diameters were calculated from Vanderveen's results.[22] The value of b'_{0-i} was taken to be 4.6×10^{-3}. The theoretically proper practice of including

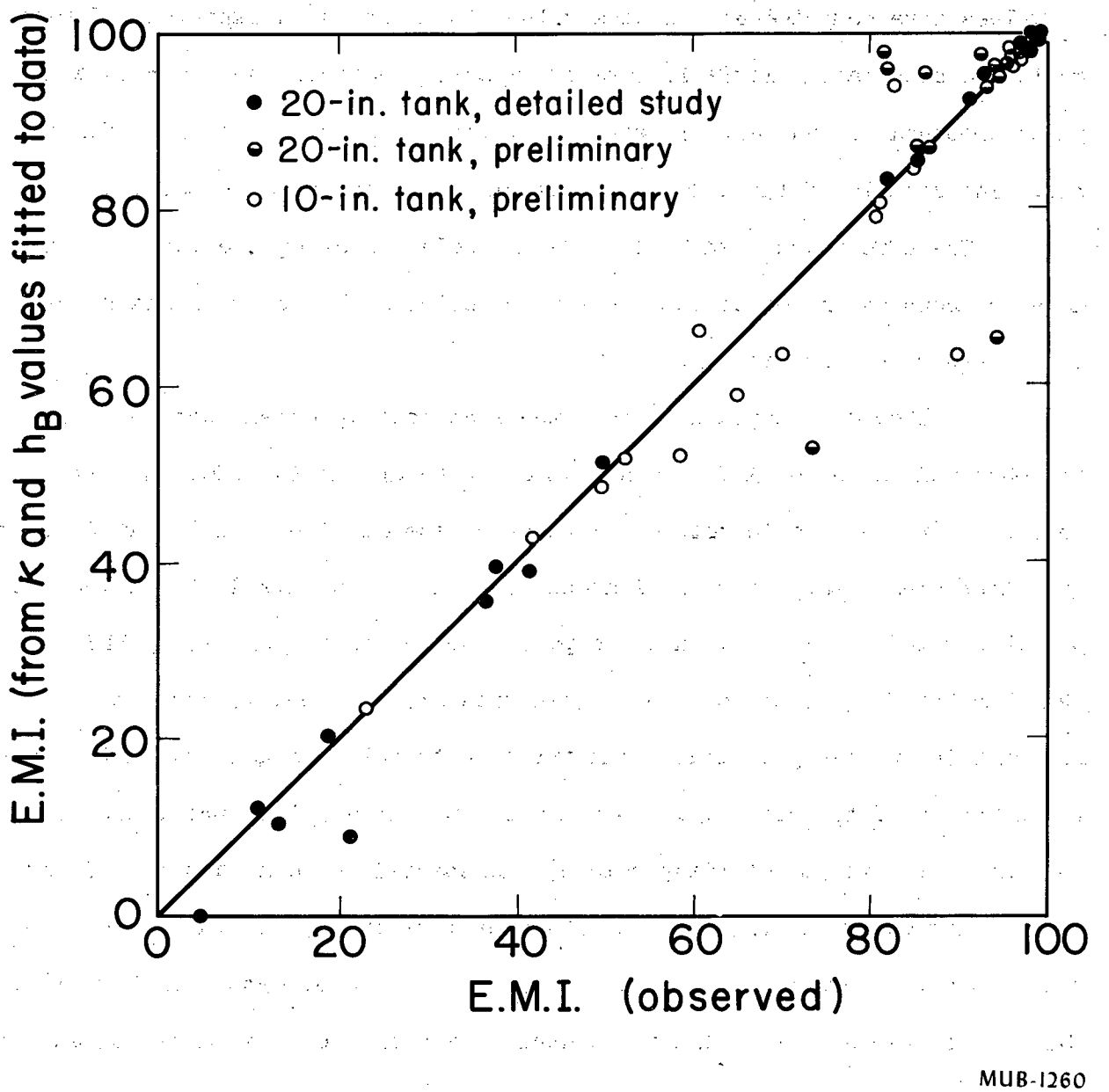

Fig. 15. Smoothed-fit and observed values of EMI.

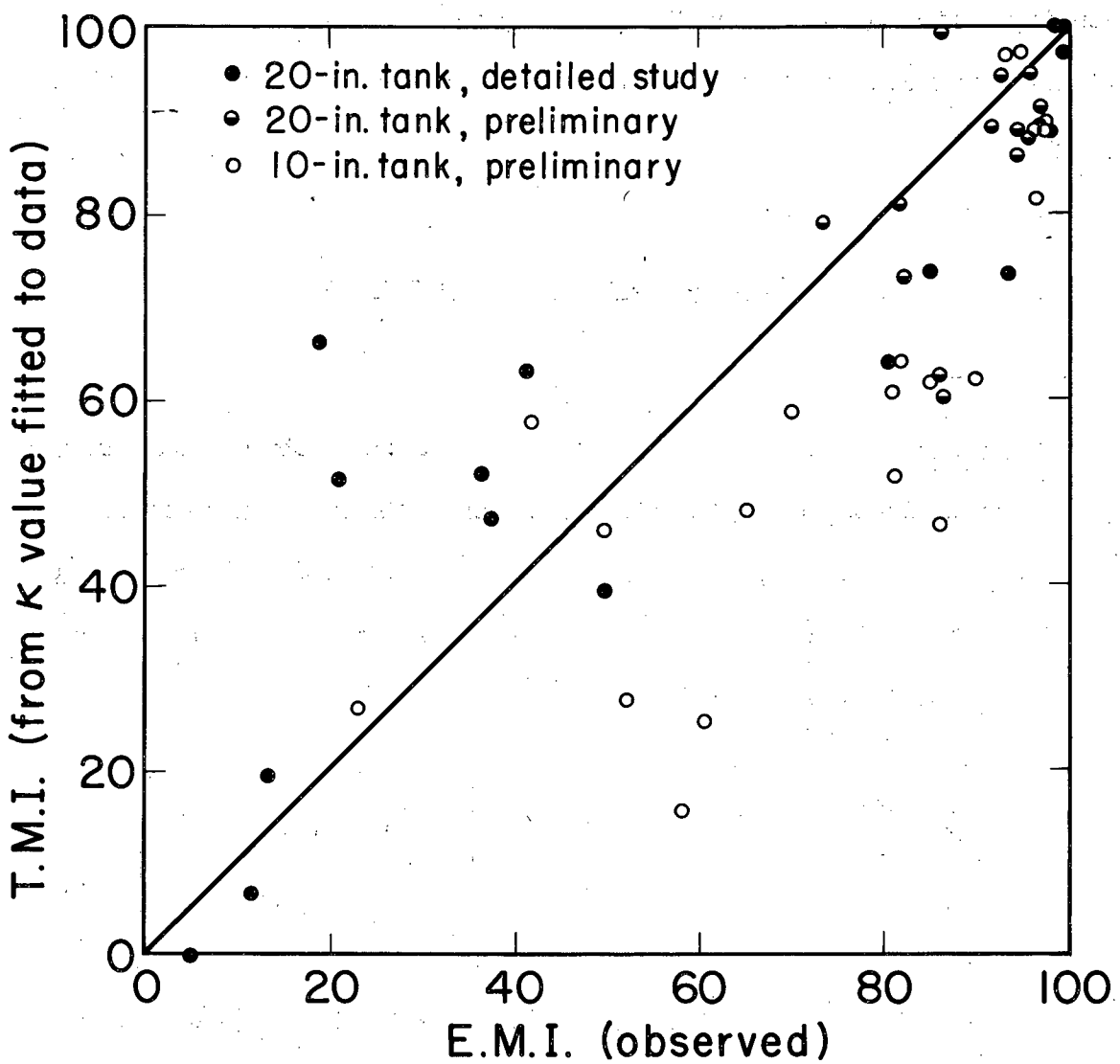

MUB-1261

Fig. 16. Comparison of TMI and observed EMI.

the density ratio $\rho/\Delta\rho$ in the Froude group was followed, as well as the additional modification of the denominator by the volume-fraction of the continuous phase.

C. Correlations for the Parameters

1. Result for κ

The computed values for κ and for the dimensionless groups suggested by the theoretical analysis (Eq. 30) are shown in Table V (Appendix 1). κ was correlated with these groups, by using a standard linear-regression program (written by R. S. Brown) on the IBM 650. The optimum result, which has a correlation coefficient of 0.83, is:

$$\ln \kappa = 3.39 \pm 1.09 - (0.232 \pm 0.040) \ln \left[N_{Fr}^{3} \left(\frac{L}{d_p} \right)^2 N_{Re} \, G^{3/2} \right] . \tag{37}$$

The use of a 3:2:1 ratio of the exponents for N_{Fr}, (L/d_p), and N_{Re}, respectively, was suggested by the results of earlier trial regressions. It also allows the more logical choice of the average droplet diameter as the characteristic length (replacing the impeller diameter) in the dimensionless groups.

Since the theoretical model for κ was based upon a ratio of squared velocities (Eq. 22), the coefficient of the independent variable in Eq. (37) should be 2/7, which is slightly beyond the prediction interval, to satisfy the model exactly. A relation of this type is shown in Fig. 17 as a solid line with the following analytical form:

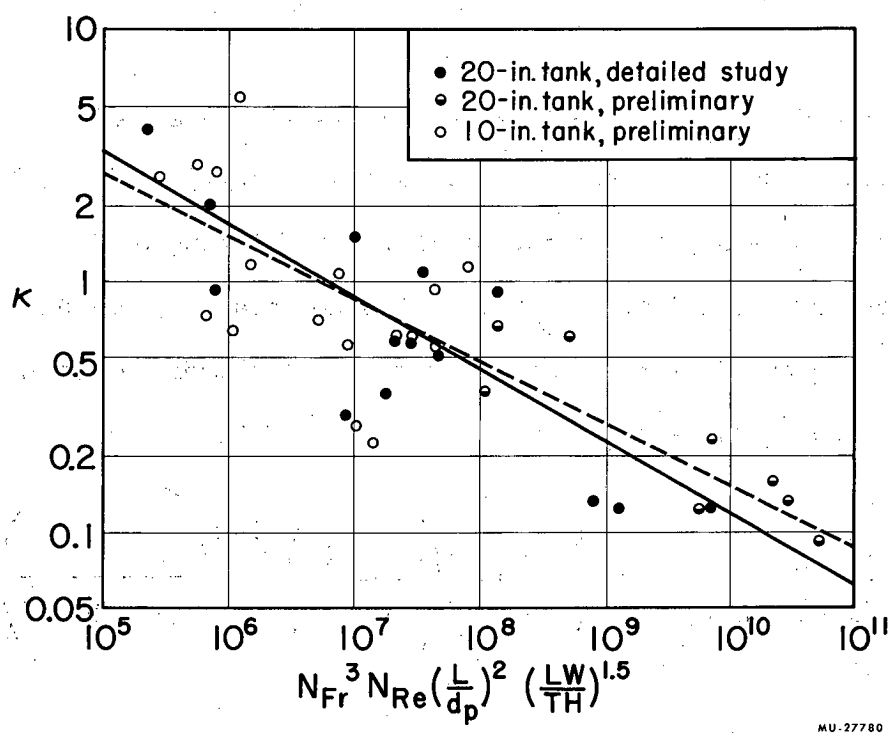

Fig. 17. Correlation for κ .

$$\kappa = 88\left[\left(\frac{N^2L^2\,\bar{\rho}}{d_p g(1-\bar{\phi})\,|\Delta\rho|}\right)^3\left(\frac{NL\,d_p\,\bar{\rho}}{\mu_m}\right)\left(\frac{LW}{TH}\right)^{3/2}\right]^{-2/7}$$

$$= 88\left[(N_{Fr})^3\;N_{Re}\;(L/d_p)^2\;G^{3/2}\right]^{-2/7}\;. \qquad (38)$$

By equating the exponent for each of the dimensionless groups in (38) with the respective exponent in the theoretical model (Eq. 30), it will be seen that the latter is exactly satisfied with $n = 4/7$ throughout.

In order to eliminate d_p from this correlation, we can apply Eq. (2) with a numerical factor of 2 to account for the average extent of coalescence. Thus, Eq. (38) becomes

$$\kappa = 25\left[\left(\frac{N^2L\,\bar{\rho}}{(1-\bar{\phi})g\,|\Delta\rho|}\right)^3\left(\frac{NL^2\,\bar{\rho}}{\mu_m}\right)\left(\frac{N^2L^3\,\bar{\rho}}{\sigma}\right)^{1.2}\left(\frac{1}{(1+2.5\,\phi)^2}\right)\left(\frac{LW}{TH}\right)^{3/2}\right]^{-2/7}. \qquad (39)$$

The dashed line in Fig. 17 represents a slightly rounded form of the optimum statistical result:

$$\kappa = 48\left[\left(\frac{N^2L^2\,\bar{\rho}}{d_p\,g(1-\bar{\phi})\,|\Delta\rho|}\right)^3\left(\frac{NL\,d_p\,\bar{\rho}}{\mu_m}\right)\left(\frac{LW}{TH}\right)^{3/2}\right]^{-1/4}. \qquad (40)$$

Of these two relationships, Eq. (38) is somewhat preferred because of its greater theoretical significance.

A few data points from the preliminary studies, observed at high mixing speeds, were dropped from Fig. 17, because of strong evidence that centrifugation effects occurred that were not considered in the models developed here. Under conditions of centrifugation, $\emptyset_s$ would not be expected to be independent of radial position, nor to follow a distribution with height based on a gravitational settling model.

2. Result for h_B

The values of $h_B/\overline{\emptyset}$ from Table V (Appendix 1) were correlated with the parameters of Eq. (32), again using linear regression on the IBM 650. The large number of runs for which $h_B/\overline{\emptyset}$ was zero could not be included in the regression. The form of the dependent variable was chosen as $h_B/\overline{\emptyset}$, rather than h_B, to normalize the range of values for it between 0 and 1.

The initial regression runs showed h_B to be almost completely insensitive to N_{Re}. Moreover, N_{Fr} was less effective in reducing the residual variance than N_{We}, although a reasonably high correlation coefficient (0.71) was obtained by using only N_{Fr} and G.[24] As the end result, a regression equation with N_{We} and G was established, having a correlation coefficient of 0.79:

$$\frac{h_B}{\overline{\emptyset}} = 1.683 \pm 0.663 - (0.271 \pm 0.066)\ln N_{We} - (0.194 \pm 0.132)\ln G . \tag{41}$$

A separate regression of this same form for the results of the detailed studies had an intercept value of 0.530 ± 1.226, a coefficient for $\ln N_{We}$ equal to -0.365 ± 0.103, and a correlation coefficient of 0.94. This result, in conjunction with the values of N_{We} corresponding to the zero-value $h_B/\overline{\emptyset}$

points, justified rounding Eq. (41) to the form shown in Fig. 18. The preferred correlation thus becomes

$$\frac{h_B}{\bar{\phi}} = -1.39 \log_{10} (N_{We} G^{0.7}) + 2.31 . \qquad (42)$$

Although the foregoing equation is quite convenient, it is not known whether $h_B/\bar{\phi}$ is a theoretically more appropriate form than h_B alone. For this reason, a relation for the latter was derived directly from (42) which should be equally accurate:

$$h_B = 0.28 \log_{10} \left[N_{We} (G)^{0.7} \bar{\phi}^{-1} \right] + 0.66. \qquad (43)$$

D. Conditions for Occurrence of Kappa Control

Since the presence of a stagnant layer of material in an agitator adversely affects the capacity and performance of the process, it is generally essential to choose agitation parameters for Eq. (42) which will give $h_B = 0$. However, it is also necessary to choose κ smaller than the limiting value (Fig. 4) that will give $\phi_{max} = 0.70$, in order to avoid having kappa control of h_B.

To provide a basis for determining whether the agitation is dispersion-controlled or kappa-controlled, the criterion for $h_B = 0$ is substituted into Eq. (42) and the result rewritten as

$$N^2 = 38 \sigma/L^3 \bar{\rho} \; G^{0.7} . \qquad (44)$$

Equation (39) can be similarly rewritten:

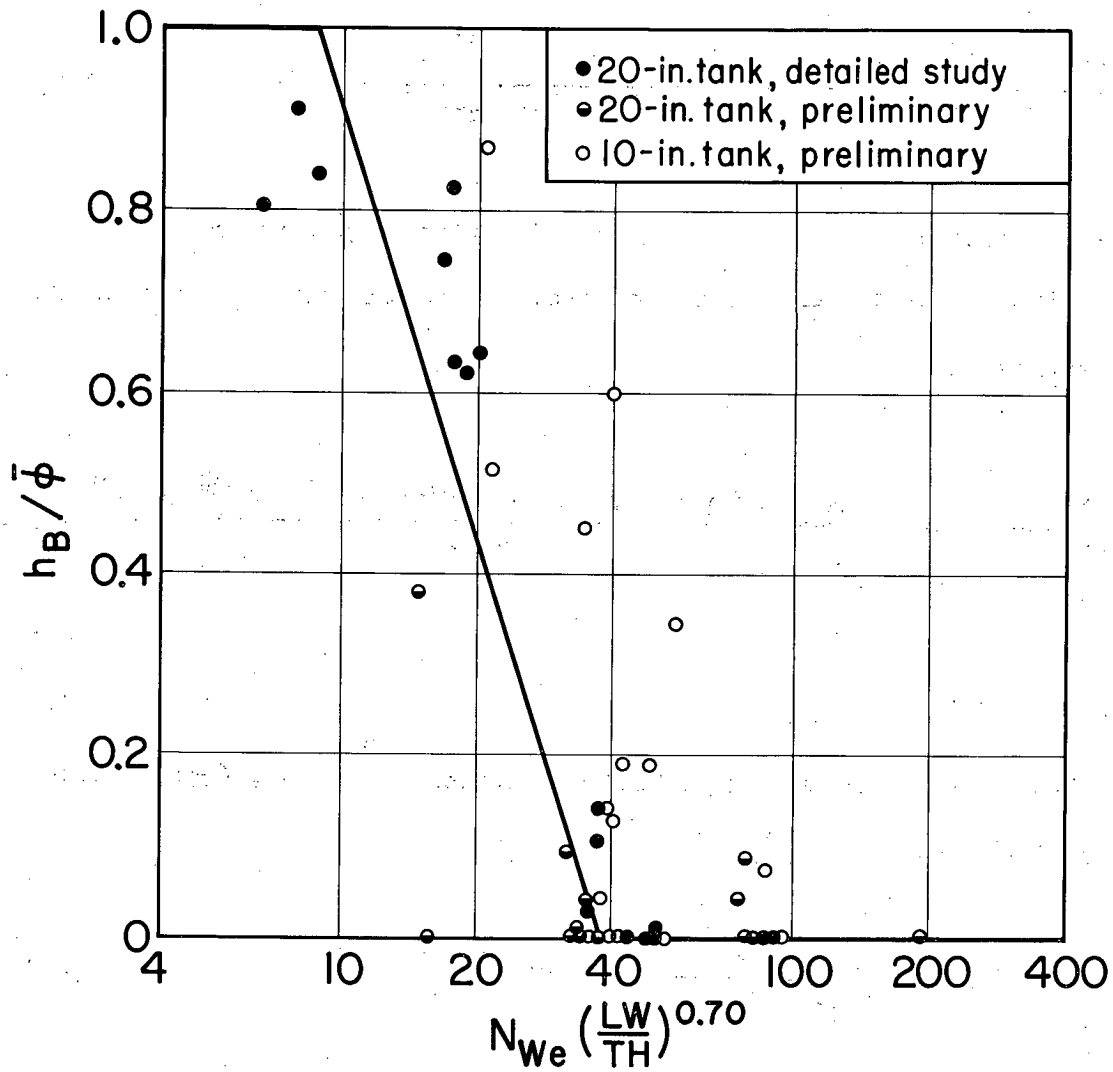

MUB-1262

Fig. 18. Correlation for h_B/ϕ .

$$N^2 = \frac{11(1 - \bar{\phi})^{0.64} (1 + 2.5\,\bar{\phi})^{0.43} (g|\Delta\rho|)^{0.64} \mu_m^{0.21} \sigma^{0.26}}{\kappa^{0.75} L^{1.83} \bar{\rho}^{1.11} G^{0.32}} , \qquad (45)$$

where κ is determined from Fig. 4, as a function of $\bar{\phi}$, to assure that $h_B = 0$ of the system is under kappa control. Equating the two expressions for N^2 results in

$$\frac{\phi^{0.74} \bar{\rho}^{0.11}}{|\Delta\rho|^{0.46} \mu_m^{0.21}} = \frac{0.29(1 - \bar{\phi})^{0.64} (1 + 2.5\,\bar{\phi})^{0.43} L^{1.17} g^{0.64} G^{0.38}}{\kappa^{0.75}} = C . \qquad (46)$$

This may be further simplified by setting $\bar{\rho}^{0.11} \approx 1$ (within ± 10% for the range 0.42 to 2.36 g/cm^3):

$$\frac{\sigma^{3.5}}{|\Delta\rho|^3 \mu_m} = 0.01\, C^{4.8} , \qquad (47)$$

where $g = 980$ cm/sec^2, L is in cm, σ in dynes/cm, $|\Delta\rho|$ is in g/cm^3, and μ_m is in centipoises (cP).

The criterion represented by the right-hand term in Eq. (47), which is a constant for any given system, has been derived to represent the condition where kappa control and dispersion control both give exactly $h_B = 0$. If the two sides of (47) are not equal, the inequality has the following interpretation:

If $\sigma^{3.5}/|\Delta\rho|^3 \mu_m$ is less than the constant term, the behavior of the system can be calculated entirely from kappa-control considerations.

The opposing case, where $\sigma^{3.5}/|\Delta\rho|^3 \mu_m$ is greater than the constant term, is now discussed. Figure 19 shows the ratio of the agitator speed at any given $h_B/\bar{\phi}$ to the speed that would give $(h_B/\bar{\phi}) = 0$, for both dispersion control and kappa control. The dispersion-controlled curve is taken directly from Fig. 18, while the kappa-controlled curves have been derived from the intercept values at $\bar{\phi}_{max} = 0.7$ in Figs. 6 through 8, together with Eq. (39)—or its equivalent, $\kappa N^{2.70} = \text{const.}$).

Since each curve is plotted on its own relative-speed scale, replotting on an absolute-speed scale in any actual situation would always have the kappa-controlled curves displaced to either the right or the left of the dispersion-controlled curve. Whichever curve lies above the other will control the mixing behavior. Thus, at the lowest speeds, dispersion will always control. If the dispersion-controlled curve intersects the kappa-controlled curve, the system will shift to the latter as the speed increases. Then, because of the convex shape of kappa-controlled curves, it is even possible to shift back to dispersion control before h_B reaches zero.

The extreme speed ratio between the relative-speed curves for the two cases is seen to occur at $h_B/\bar{\phi} = 0.75$, where it is $6.0/3.33 = 1.80$. For this reason, a combination of kappa control and dispersion control will be encountered in systems where the group $\sigma^{3.5}/|\Delta\rho|^3 \mu_m$ is only moderately greater than the constant term in Eq. (46). In order to have the system entirely in dispersion control, it would probably be necessary that $[\sigma^{3.5}/(|\Delta\rho|^3 \mu_m)] > 2.8\, C^{4.8}$. As an indication of the restrictiveness of this inequality, for the geometry of the detailed studies with the kerosene-water system, at $\bar{\phi} = 0.1$, we had

$$[\sigma^{3.5}/(|\Delta\rho|^3\mu_m)] = 6.3 \times 10^7 > 2.8\, C^{4.8} = 2.2 \times 10^5 .$$

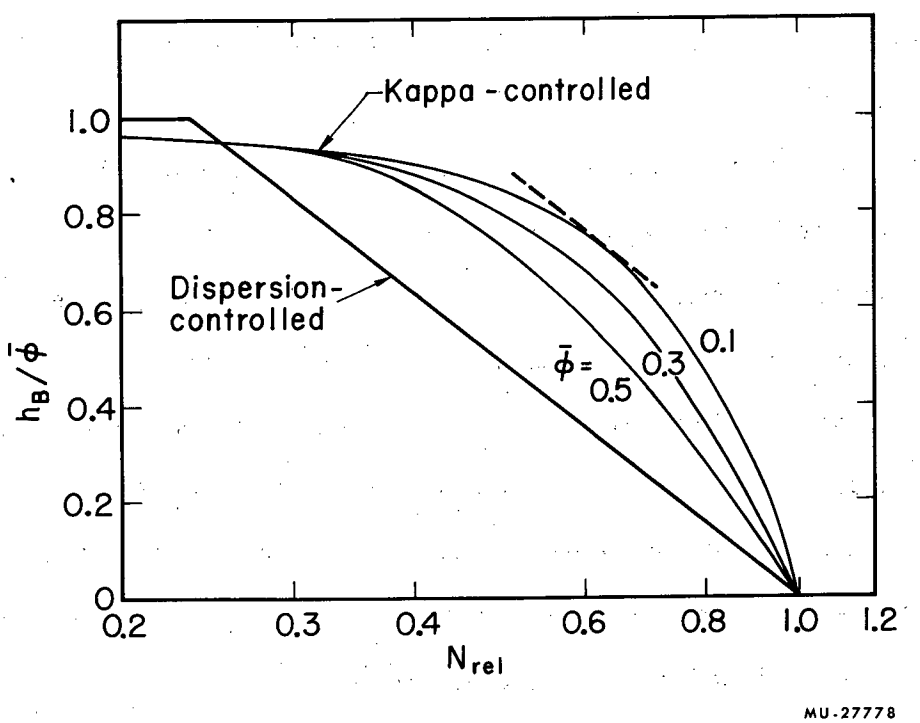

Fig. 19. Relative effect of agitator speed in the two types of h_B control.

E. Comparison With Results of Other Investigators

The mixing-criterion relations reported in the Introduction, Eqs. (5) through (9), and (11), were seen to involve the Reynolds number, Froude number, impeller-diameter/particle-size ratio, and geometric factors. In Table IV, these relations are recast into the general form of Eq. (30), enabling the different results to be compared on a fairly uniform basis.

When n is greater than 0.5, the effect of the Reynolds number is for an increase in continuous-phase viscosity to hinder the attainment of homogeneity. Below 0.5 the opposite effect applies.

The slurry-height criterion of Weisman and Efferding is analogous to the behavior of the curve for $\kappa = 10$ in Fig. 5. It appears that neither their criterion, nor that of Pavlushenko for liquids, is very closely related to the κ behavior noted by the present authors. However, the criterion of Zwietering, and also the one used by Oyama and Endoh, seems to correspond closely to κ. It also seems likely that measurements in unbaffled tanks, which have not yet been made, would show a lower n value in the vicinity of Pavlushenko's and Nagata's criteria for such vessels.

Table IV. Comparison of homogeneity criteria.

Investigator	Dispersed phase	n value from N_{Re} or N_{Fr}	n value from L/d_p
	Baffled tanks		
Zwietering[a]	Solid	0.55	0.60
Oyama-Endoh[b]	Solid	0.50	0.61
Weisman-Efferding[c]	Solid	0.33	0.44
Pavlushenko et al.[d]	Liquid	0.81	0.61[e]
This study	Liquid	0.57	0.57
	Unbaffled tanks		
Pavlushenko et al.[f]	Solid	0.40	0.53
Nagata[g]	Solid	0.44	0.56

[a]See reference 29.

[b]See reference 13.

[c]See reference 25.

[d]See reference 15.

[e]N_{We} effect is recomputed by assuming $\frac{L}{d_p} \propto N_{We}^{0.60}$ (neglecting coalescence effects).

[f]See reference 14.

[g]See reference 10.

VI. APPLICATIONS

Since the two-parameter exponential model seems to offer a realistic description of the dispersed-phase distribution in an agitated emulsion, it is of interest to consider some applications of the model. It is possible to test the extent to which bulk homogeneity may be achieved in existing equipment, and to develop design criteria that will ensure uniform suspensions in new equipment.

A. Testing An Existing Process

If the operation of an existing agitator is unsatisfactory because of poor interphase contact, improvement can usually be obtained by achieving a more uniform emulsion. However, it is first necessary to ascertain the extent and type of non-uniformity. The following procedure outlines the necessary steps for this application of the model:

(a) Calculate κ from Eq. (38).

(b) From Fig. 4, determine whether the mixing is in the dispersion-controlled or the coalescence-controlled region.

(c) If dispersion is the controlling mechanism, calculate h_B from Eq. (42), and $\overline{\phi}_{max}$ from Eq. (36) or Figs. 6, 7, and 8.

(d) If coalescence is the controlling mechanism, set $\overline{\phi}_{max} = 0.70$ and calculate h_B from Eq. (34).

B. Design of Equipment

The capacity of an agitator can readily be determined from production requirements. However, the optimum choice of an impeller is governed by the following criteria:

(a) for power consumption,[16]

$$N^3 L^4 W = \text{a minimum};$$

(b) for drop diameter, determined by turbulent breakup,[2]

$$N^{1.2} L^{0.8} \geq \text{a constant};$$

(c) for drop diameter, determined by coalescence,[22]

$$N^{0.65} L^{-0.15} \geq \text{a constant};$$

(d) for uniformity within the dispersion (Eq. 38),

$$N^{2.7} L^{2.9} W^{0.43} \geq \text{a constant; and}$$

(e) for elimination of the unmixed phase (Eq. 42),

$$N^2 L^{3.7} W^{0.7} \geq \text{a constant.}$$

Some two of conditions (b) through (e) will be found to control the design; in those conditions the equality will apply, while the remaining two will be overdesigned. Since the primary purpose of this paper is to explore bulk homogeneity, let conditions (d) and (e) be considered, for illustrative purposes. The first objective is to determine the optimum values of L and W; combining (d) and (e) gives:

$$N^3 L^{1.7} W^{0.10} = \text{a constant,}$$

and combination of this with (a) results in:

$$L^{2.6} W = \text{a minimum.}$$

Since the impeller-tip speed (π NL) is proportional to the shear rate within the emulsion, it may be more desirable to minimize power by reducing W rather than L. The suitability of a rotating-disc impeller for some applications is thus at least partially explained.

VII. CONCLUSIONS

The following conclusions from this work may now be presented:

(1) A two-parameter exponential model for the distribution of the dispersed-phase in liquid-liquid agitation provides a criterion for establishing bulk homogeneity that is independent of the specific objective of the contacting process.

(2) The inhomogeneity parameter, κ , is dependent upon the impeller dimensions, stirring speed, volume-fraction of the dispersed phase, density of each phase, viscosity of each phase, and the interfacial area produced, for vessels of different sizes but similar proportions.

(3) The elimination of an undispersed layer is dependent upon the average volume-fraction of the dispersed phase, the impeller dimensions, the stirring speed, and the interfacial tension between phases, for vessels of different sizes but similar proportions.

(4) In fully baffled agitators, the dispersed-phase volume-fraction at any point is dependent upon fractional tank height, and independent of radial or angular location.

(5) A value of 0.10 is sufficiently small for κ to ensure deviations of less than 5% in the local volume fraction from the overall average and to ensure dispersion control of h_B , the height of the undispersed layer, if any.

(6) At values of κ less than 0.10, centrifugation effects become important.

(7) When a stagnant layer of the dispersible phase is present ($h_B > 0$), either coalescence or lack of dispersion may be the cause, depending upon the values of the interfacial tension, density difference, mixture viscosity, average-volume fraction, and the impeller diameter, for vessels of different sizes but similar proportions.

(8) The conclusions drawn appear to offer a sound engineering basis for the design of liquid-liquid agitation equipment.

ACKNOWLEDGMENTS

A portion of this study was carried out while the principal author (LHW) was a National Science Foundation Fellow. Further financial assistance, as well as research and computation facilities, were supplied by the Lawrence Radiation Laboratory under the auspices of the U.S. Atomic Energy Commission.

The authors are grateful for advice from E. F. Orlemann and C. J. Vogt.

The contents of this report have been filed by one of the authors (LHW) as a thesis in partial fulfillment of the requirements for the Master of Science Degree in the Graduate Division, University of California, Berkeley, California.

APPENDICES

1. Computation Procedure and Tabulated Results

A. Computations for each point:

(1) Dispersed-phase volume fraction $\phi_{s,j}$;

(2) Continuous-phase volume fraction $\phi_{c,j}$;

(3) M. N. from Eq. (12);

(4) $i_{m,j}$ from M. N. and the conditions

$$i_{m,j} \leq 100 , \qquad \text{(a)}$$

$$i_{m,j} = \text{M. N. or } i_{m,j} = 200 - \text{M. N.} \qquad \text{(b)}$$

B. Computations for each height:

(1) $$\phi_{av} = \frac{1}{q} \sum_{j=1}^{q} \phi_{s,j} ;$$

(2) $$i_{m,av} = \frac{1}{q} \sum_{j=1}^{q} i_{m,j} .$$

C. Computations for each run:

(1) $$\text{EMI (obs)} = \frac{1}{q} \sum_{j=1}^{q} i_{m,j} ;$$

(2) κ from a data-smoothing procedure as follows:

(a) Discard all values of $\phi_{av} \geq 0.70$;

(b) Calculate $k_i = \dfrac{\ln \phi_{av,h_i} - \ln \phi_{av,h_{i+1}}}{h_{1+1} - h_i}$

for remaining values of ϕ_{av} ;

(c) $\kappa = \frac{1}{a} \sum_{i=1}^{a} k_i$.

(3) The intercept at $h = 0$, ϕ_{lim} , from the slope of the semilog fit of the data:

(a) $\ln \phi_{av} = \frac{1}{a} \sum_{i=1}^{a} \ln \phi_{av,i}$;

(b) $\bar{h} = \frac{1}{a} \sum_{i=1}^{a} h_i$;

(c) $\ln \phi_{lim} = \ln \phi_{av} + \kappa \bar{h}$.

(4) h_B from the values of κ , ϕ_{lim} , and $\bar{\phi}$ using the following derivation of the material balance (Eq. 17):

$$\bar{\phi} = h_B + \int_{h_B}^{1.0} f(h)\, dh \; ; \qquad \text{(I)}$$

$$f(h) = \phi_{max}\, e^{-\kappa\,(h-h_B)} \;; \qquad \text{(II)}$$

$$\phi_{max} = \phi_{lim}\, e^{-\kappa h_B} \;. \qquad \text{(III)}$$

Substitution of (III) and (II) into (I), and integrating, gives

$$\bar{\phi} = h_B + \frac{\phi_{lim}}{\kappa}\left[e^{-\kappa\, h_B} - e^{-\kappa}\right] . \qquad \text{(IV)}$$

Equation (IV) was then used to solve for h_B by an iterative technique.

(5) ϕ_{max} from Eq. (III) and the calculated values of κ, ϕ_{lim}, and h_B.

(6) Each of the dimensionless groups used in the regression analyses was computed using the defining relations:

$$N_{We} = \frac{N^2\, L^3\, \bar{\rho}}{\sigma} \;;$$

$$N_{Re} = \frac{N L^2\, \bar{\rho}}{\mu_m} \;;$$

$$N_{Fr} = \frac{N^2\, L\, \bar{\rho}}{g\, |\Delta\, \rho|\,(1 - \bar{\phi})} \;;$$

$$G = \frac{LW}{TH} \;;$$

$$\frac{d_p}{L} = 0.055\, N_{We}^{-0.60}\,(1 + 2.5\,\bar{\phi}) + (4.6 \times 10^{-3}) N_{We}^{-0.45} N_{Re}^{0.25}\, \Psi^{-0.70}\, \bar{\phi}^{0.30} \;,$$

where $\Psi = \frac{\mu_c}{\mu_d} (1 - \emptyset)^{2.5} + \frac{\mu_d}{\mu_c} \bar{\emptyset}^{2.5}$.

The average physical properties used are defined as:

$$\bar{\rho} = \rho_c + \bar{\emptyset} (\rho_d - \rho_c) ;$$

$$\mu_m = \frac{\mu_c}{(1 - \bar{\emptyset})^{3/2}} \left[1 + \frac{\bar{\emptyset} (\mu_d - \mu_c)}{\mu_c + \mu_d} \right]^{3/2} .$$

(7) From the fitted constants, κ , $\emptyset_{max}$, and h_B , smoothed values for $\emptyset_{s,j}$, $i_{m,j}$, $\emptyset_{av}$, $i_{m,av}$ and EMI (smoothed fit), were calculated by the procedures outlined above in (A), (B), and (C-1).

Table V. Fitted parameters and correlating groups.

System	N (rps)	$\bar{\phi}$	L (in.)	G ($\times 10^2$)	N_{Re} ($\times 10^{-4}$)	N_{We} ($\times 10^{-3}$)	N_{Fr}	$\frac{dp}{L}$ ($\times 10^3$)	ϕ_{lim}	ϕ_{max}	κ	$f(\kappa)$ ($\times 10^{-5}$)[a]	$hB/\bar{\phi}$	$f\left(\frac{h_B}{\bar{\phi}}\right)$[b]	EMI(obs) (%)	EMI(s.f.) (%)	TMI (%)
(10-in. tank, preliminary studies)																	
H_2O in CCl_4	2.83	0.10	5.00	5.42	6.06	0.665	0.295	3.71	0.090	0.085	1.184	14.2	0.516	21.7	49.6	48.6	45.8
	4.50	0.10	5.00	5.42	9.63	1.68	0.745	2.52	0.117	0.113	1.156	794.	0.345	54.9	86.0	89.2	46.4
	2.83	0.20	5.00	5.42	4.87	0.639	0.319	5.01	0.130	0.080	2.752	7.84	0.869	20.8	23.0	23.5	26.6
	4.50	0.20	5.00	5.42	7.75	1.61	0.806	3.42	0.341	0.341	0.933	431.	0.000	52.6	81.1	80.6	51.7
	4.50	0.40	5.00	5.42	4.62	1.48	0.987	5.17	0.481	0.459	0.611	211.	0.190	48.3	89.9	63.3	62.1
	1.83	0.10	7.50	8.18	8.86	0.946	0.185	3.29	0.742	0.742	5.438	12.0	0.000	41.2	57.9	52.1	15.5
	1.83	0.20	7.50	8.18	7.13	0.908	0.200	4.48	0.136	0.125	0.738	6.56	0.597	39.5	42.1	42.6	57.5
	2.83	0.20	7.50	8.18	11.0	2.17	0.479	3.17	0.297	0.297	0.617	280.	0.000	94.3	85.0	84.4	61.8
	2.83	0.40	7.50	8.18	6.57	2.00	0.587	4.77	0.428	0.426	0.227	136.	0.073	87.0	96.3	97.1	81.5
	1.83	0.10	6.77	12.2	7.18	0.690	0.167	3.73	0.171	0.171	0.644	10.0	0.000	39.0	80.8	79.1	60.8
	1.83	0.20	6.77	12.2	5.78	0.663	0.181	5.03	0.613	0.598	2.959	5.53	0.043	37.5	60.4	66.3	25.3
	1.83	0.40	6.77	12.2	3.44	0.610	0.221	7.58	1.038	0.649	2.605	2.72	0.451	34.5	52.1	51.8	27.7
MIBK in H_2O	2.83	0.30	5.00	5.42	2.84	1.28	0.702	4.96	0.367	0.352	0.707	49.8	0.192	41.7	70.0	63.4	58.6
	2.83	0.50	5.00	5.42	1.79	1.23	0.942	5.00	0.796	0.742	1.088	73.8	0.129	40.1	65.0	58.8	47.9
H_2O in MIBK	2.83	0.30	5.00	5.42	3.54	1.17	0.643	3.68	0.356	0.347	0.560	87.5	0.142	38.1	83.0	93.9	64.1
(20-in. tank, preliminary studies)																	
White oil in H_2O	6.83	0.20	5.00	2.50	5.88	1.94	5.98	0.989	0.214	0.214	0.091	5.10×10^5	0.000	36.9	97.0	97.3	91.6
	4.50	0.40	5.00	2.50	1.95	0.818	3.37	2.18	0.539	0.539	0.608	6.08×10^3	0.000	15.5	85.4	87.0	62.2
	6.83	0.40	5.00	2.50	2.97	1.89	7.77	1.38	0.430	0.430	0.132	2.90×10^5	0.000	35.9	95.7	96.6	88.4
	6.83	0.60	5.00	2.50	1.29	1.84	11.3	1.83	0.640	0.638	0.158	2.15×10^5	0.038	35.0	94.5	96.2	86.3
	1.83	0.20	10.00	5.00	6.30	1.11	0.858	-	0.222	0.222	0.027	-	0.000	34.2	93.5	93.7	97.3
	2.83	0.20	10.00	5.00	9.74	2.66	2.05	-	0.219	0.219	0.026	-	0.000	81.9	94.8	94.8	97.5
	1.83	0.40	10.00	5.00	3.18	1.08	1.12	1.89	0.546	0.545	0.660	1.36×10^3	0.003	33.3	86.4	87.0	60.2
	2.83	0.40	10.00	5.00	4.92	2.59	2.67	-	0.421	0.421	0.054	-	0.000	79.8	95.8	96.8	94.9
	1.83	0.60	10.00	5.00	1.38	1.06	1.63	-	0.621	0.621	0.053	-	0.000	32.7	92.7	97.3	95.0
	2.83	0.60	10.00	5.00	2.14	2.53	3.90	1.58	0.616	0.612	0.123	5.58×10^4	0.088	78.0	94.5	65.3	89.0
H_2O in white oil	4.50	0.20	5.00	2.50	0.0862	0.778	2.40	2.14	0.154	0.151	0.267	101.	0.380	14.8	73.3	52.8	78.9
	1.83	0.20	10.00	5.00	0.140	1.03	0.793	-	0.185	0.185	0.005	-	0.094	31.7	86.2	95.2	99.5
	2.83	0.20	10.00	5.00	0.217	2.46	1.90	1.22	0.231	0.230	0.366	1.08×10^3	0.044	75.8	82.2	95.8	73.2
	4.50	0.20	10.00	5.00	0.345	6.22	4.80	0.787	0.207	0.206	0.237	6.86×10^4	0.000	192.	81.6	97.6	80.8

Table V (continued)

System	N (rps)	$\bar{\phi}$	L (in.)	G ($\times 10^2$)	N_{Re} ($\times 10^{-4}$)	N_{We} ($\times 10^{-3}$)	N_{Fr}	$\frac{d_p}{L}$ ($\times 10^3$)	ϕ_{lim}	ϕ_{max}	κ	$f(\kappa)$ ($\times 10^{-5}$)[a]	$hB/\bar{\phi}$	$f\left(\frac{h_B}{\phi}\right)$[b]	EMI(obs) (%)	EMI(s.f.) (%)	TMI (%)
(20-in. tank, detailed studies)																	
Kerosene in H_2O	1.83	0.10	6.67	3.33	4.08	0.363	0.322	3.40	0.734	0.226	2.03	7.11	0.839	8.43	11.2	12.0	6.7
	2.83	0.10	6.67	3.33	6.31	0.868	0.770	2.22	0.066	0.062	1.116	346.	0.643	20.1	37.5	39.6	47.3
	4.50	0.10	6.67	3.33	10.0	2.20	1.95	-	0.100	0.100	0.000	-	0.000	51.1	99.3	100.0	100.0
	1.83	0.20	6.67	3.33	-	-	-	-	-	-	-	-	1.000	-	4.7	0.0	0.0
	2.83	0.20	6.67	3.33	4.86	0.850	0.848	2.93	0.116	0.107	0.583	207.	0.632	19.7	41.3	39.2	63.2
	4.50	0.20	6.67	3.33	7.73	2.15	2.15	1.93	0.211	0.211	0.122	1.23×10^4	0.007	49.9	97.0	98.5	89.1
	1.83	0.40	6.67	3.33	1.74	0.341	0.454	6.75	0.698	0.156	4.105	2.13	0.912	7.92	13.3	10.4	19.6
	2.83	0.40	6.67	3.33	2.69	0.816	1.09	4.58	0.499	0.341	1.537	98.9	0.620	18.9	49.7	51.3	39.4
	4.50	0.40	6.67	3.33	4.28	2.06	2.76	-	0.400	0.400	0.000	-	0.000	47.8	98.9	100.0	100.0
	1.83	0.40	10.00	5.00	3.92	1.16	0.682	4.01	0.455	0.454	0.294	84.6	0.026	35.7	93.3	95.0	77.3
	2.83	0.40	10.00	5.00	6.08	2.76	1.62	-	0.410	0.410	0.029	-	0.000	85.1	99.5	99.2	97.2
	1.83	0.21	10.00	5.00	6.91	1.20	0.541	2.63	0.249	0.247	0.358	177	0.105	37.0	85.1	84.8	73.7
	2.83	0.21	10.00	5.00	10.7	2.87	1.29	1.78	0.228	0.228	0.131	8.12×10^3	0.000	88.4	98.3	97.6	88.4
	1.83	0.12	10.00	5.00	8.78	1.23	0.494	2.04	0.144	0.143	0.560	284.	0.142	37.9	81.8	83.3	64.1
	4.50	0.12	5.00	2.50	5.40	0.927	1.49	2.25	0.038	0.035	0.919	1.39×10^3	0.825	17.6	36.4	35.5	52.1
	6.83	0.12	5.00	2.50	8.20	2.14	3.44	1.53	0.124	0.124	0.120	5.62×10^4	0.000	40.7	91.7	92.4	89.3
	2.83	0.40	5.00	2.50	1.52	0.347	0.817	6.54	0.110	0.033	0.934	7.67	0.804	6.60	21.2	8.2	51.6
	4.50	0.40	5.00	2.50	2.42	0.877	2.07	4.30	0.242	0.208	0.510	467.	0.743	16.7	18.7	20.4	66.2

a $f(\kappa) = N_{Fr}\, N_{Re} \left(\frac{L}{d_p}\right)^2 G^{3/2} = \left(\frac{N^2 L^2 \bar{\rho}}{d_p g\,(1-\bar{\phi})|\Delta\rho|}\right)^3 \left(\frac{N L d_p \bar{\rho}}{\mu_m}\right) \left(\frac{LW}{TH}\right)^{3/2}$

b $f\left(\frac{h_B}{\bar{\phi}}\right) = N_{We}\, G^{0.7} = \left(\frac{N^2 L^3 \bar{\rho}}{\sigma}\right) \left(\frac{LW}{TH}\right)^{0.7}$

2. Nomenclature

A	=	a function of geometrical factors (Eq. 10).
a	=	a constant (Eq. 14).
B	=	weight-percent of solids (Eq. 5).
b	=	a constant (Eq. 14).
b'_{o-1}	=	a geometric constant (Eq. 1).
C	=	a constant (Eq. 46).
d_i	=	mean droplet diameter at point i (cm).
d_o	=	mean droplet diameter at impeller tip (cm), $0.055\ L\ f(\bar{\phi})N_{We}^{-0.60}$
d_p	=	mean particle diameter of dispersed phase (cm).
EMI	=	I_m .
$f(x)$	=	a monotonic function of any variable x.
$f(\bar{\phi})$	=	$1 + 2.5\ \bar{\phi}$.
G	=	agitator geometry group (dimensionless, LW/TH).
g	=	acceleration of gravity, 980 cm/sec^2 .
H	=	tank height (cm).
h	=	fractional tank height (dimensionless).
h_B	=	fractional tank height of boundary between dispersible (but undispersed) phase, and emulsion.
h_s	=	fractional tank height of slurry.
I_m	=	overall mixing index, $\frac{100}{q} \sum_{i=1}^{q} \frac{\phi_{s,i}}{\bar{\phi}}$.
i_m	=	local value of mixing index.
K	=	a constant.
L	=	impeller diameter (cm).
M.N.	=	mixing number defined by Eq. (12).

N = stirring speed (rps).

N_{Fr} = Froude number.

N_{min} = minimum stirring speed (Eq. 10) (rev/sec).

N_{Re} = Reynolds number.

N_{rel} = relative stirring speed (Fig. 19).

N_{We} = Weber number.

n = an exponent (Eq. 30).

q = number of samples.

T = tank diameter (cm).

TMI = theoretical mixing index, $1/(1 + \kappa)$

V_j = local continuous-phase velocity.

V_s = local dispersed-phase velocity.

V_p/V'_p = average departure from sphericity.

W = impeller width (cm).

x = an exponent.

y = an exponent, $2x$

Δ'_i = coalescence correction factor (cm) $LN_{We}^{-0.45}\ N_{Re}^{0.25}\ \Psi^{-0.70}\ \bar{\phi}^{\,0.30}$.

$\Delta\rho$ = density-difference driving gravitational force (g/cm^3).

$\Delta\rho$ = $\rho_c - \rho_d$.

κ = inhomogeneity parameter.

μ_c = continuous-phase viscosity (cP).

μ_d = dispersed-phase viscosity (cP).

μ_m = mixture viscosity (cP), $\dfrac{\mu_c}{(1-\bar{\phi})^{3/2}} \left[1 + \dfrac{\bar{\phi}(\mu_d - \mu_c)}{\mu_d + \mu_c} \right]^{3/2}$.

ρ_c = continuous-phase density, (g/cm^3).

ρ_d = dispersed-phase density, (g/cm^3).

$\bar{\rho}$ = $\rho_c + \bar{\emptyset}(\rho_d - \rho_c)$.

σ = interfacial tension (dynes/cm).

$\emptyset_{max}$ = maximum volume-fraction of dispersed phase.

$\emptyset_s$ = local volume-fraction of dispersed phase.

$\bar{\emptyset}$ = bulk-average volume-fraction of dispersed phase.

$\underline{\psi}$ = viscosity-volume-fraction parameter $\frac{\mu_c}{\mu_d}(1 - \bar{\emptyset})^{2.5} + \frac{\mu_d}{\mu_c}\bar{\emptyset}^{2.5}$.

REFERENCES

1. V. A. Bordin and Y. F. Dityakin, NACA Technical Memorandum 1281 (1951). Translation from Prikladnaya Matematika i Mekhanika 13, No. 3 (1949).
2. J. L. Fick, H. E. Rea Jr., and T. Vermeulen, The Effects of Agitator Geometry in the Mixing of Liquid-Liquid Systems. University of California Lawrence Radiation Laboratory, Report UCRL-2545, April 1954 (unpublished).
3. A. W. Hixson and A. H. Tenney, Trans. Am. Inst. Chem. Engr. 31 113 (1935).
4. D. Hyman, Mixing and Agitation, in Advances in Chemical Engineering, edited by T. B. Drew (Academic Press, New York, 1962) Vol. III.
5. F. Kneule, Chem. Ing. Tech. 28, 221 (1956).
6. H. E. Lamb, Hydrodynamics, 6th Ed., (Dover Publications, New York, 1945).
7. G. E. Langlois, J. E. Gullberg, and T. Vermeulen, Rev. Sci. Instr. 25, 360 (1954).
8. S. A. Miller and C. A. Mann, Trans. Am. Inst. Chem. Engrs. 40, 709 (1944).
9. S. Nagata, I. Yamaguchi, and M. Harada, Chem. Eng. (Japan) 24, 742 (1960).
10. S. Nagata, K. Yamamoto, K. Hashimoto, and Y. Naruse, ibid., 23 595 (1959); ibid., 24, 99 (1960).
11. S. Nagata, T. Yokoyama, and H. Naka, ibid., 17 144 (1953).
12. S. Nagata, N. Yoshioka, T. Yokoyama, and D. Teramoto, Trans. Soc. Chem. Engrs. (Japan) 8, 43 (1949).
13. Y. Oyama and K. Endoh, Chem. Eng. (Japan) 20, 666 (1956).
14. I. S. Pavlushenko, N. M. Kostin, and S. F. Matveev, Zhur. Priklad. Khin. 30, 1160 (1957).
15. I. S. Pavlushenko and A. V. Yanishevskii, ibid., 31 1348 (1958).
16. H. E. Rea, Jr. and T. Vermeulen, Effect of Baffling and Impeller Geometry on Interfacial Area in Agitated Two-Phase Liquid Systems. University of California Lawrence Radiation Laboratory Report UCRL-2123, April 1953 (unpublished).

17. W. H. Rodger, V. G. Trice, and J. H. Rushton, Chem. Eng. Progr. 52 515 (1956).

18. J. H. Rushton, ibid., 48, 33, 95 (1952).

19. J. H. Rushton, E. W. Costich, and H. J. Everett, ibid., 46, 395 (1950).

20. J. P. Sachs, Ph.D. Thesis, Illinois Institute of Technology, 1952 (unpublished).

21. V. G. Trice and W. A. Rodger, A. I. Ch. E. J. 2, 205 (1956).

22. J. H. Vanderveen, Coalescence and Dispersion Rates in Agitated Liquid-Liquid Systems. University of California Lawrence Radiation Laboratory Report UCRL-8733, December 1960 (unpublished).

23. T. Vermeulen, Fluid Mixing in Heterogeneous Systems, Proceedings of the 25th Anniversary Congress, Soc. Chem. Engrs. (Japan), Nov. 5-15, 1961.

24. T. Vermeulen, G. M. Williams, and G. E. Langlois, Chem. Eng. Progr. 51, 85-F (1955).

25. J. Weisman and L. E. Efferding, A. I. Ch. E. J. 6, 419 (1960).

26. A. M. White and S. D. Summerford, Ind. Eng. Chem. 25 1025 (1933).

27. A. M. White, S. D. Summerford, E. O. Bryant, and B. E. Lukens, ibid, 24, 1160 (1932).

28. K. Yamamoto and Z. Kawahigasi, Chem. Eng. (Japan) 20, 686 (1956).

29. T. N. Zwietering, Chem. Eng. Sci. 8, 244 (1958).

This report was prepared as an account of Government sponsored work. Neither the United States, nor the Commission, nor any person acting on behalf of the Commission:

A. Makes any warranty or representation, expressed or implied, with respect to the accuracy, completeness, or usefulness of the information contained in this report, or that the use of any information, apparatus, method, or process disclosed in this report may not infringe privately owned rights; or

B. Assumes any liabilities with respect to the use of, or for damages resulting from the use of any information, apparatus, method, or process disclosed in this report.

As used in the above, "person acting on behalf of the Commission" includes any employee or contractor of the Commission, or employee of such contractor, to the extent that such employee or contractor of the Commission, or employee of such contractor prepares, disseminates, or provides access to, any information pursuant to his employment or contract with the Commission, or his employment with such contractor.